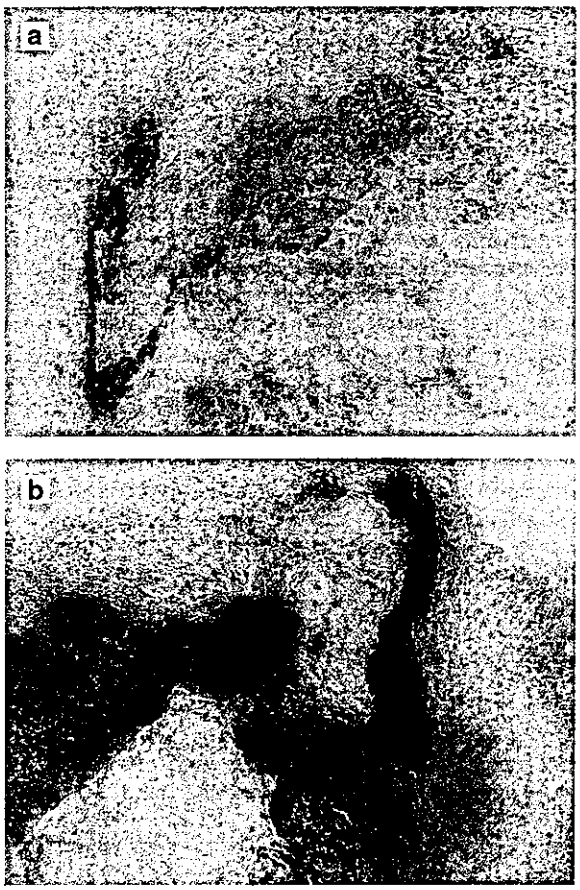

Figure 6 The effect of γ-ray irradiation on AAV-mediated transgene expression in subcutaneous tumors in BALB/c mice. The tumors were established by HEp-2 cells into the flanks of the mice xenografts. (a) Transduction with 5×10^{11} particles/tumor of AAVLacZ without γ-ray irradiation. (b) Transduction with AAVLacZ immediately after 4 Gy irradiation. Three days after AAVLacZ injection, the tumors were excised from mice and frozen in OTC embedding compound on a liquid-nitrogen bath. Cryostat sections were made and fixed with 0.05% glutaraldehyde in PBS. Histochemical staining for β-galactosidase activity was performed in the sections as described in Materials and methods.

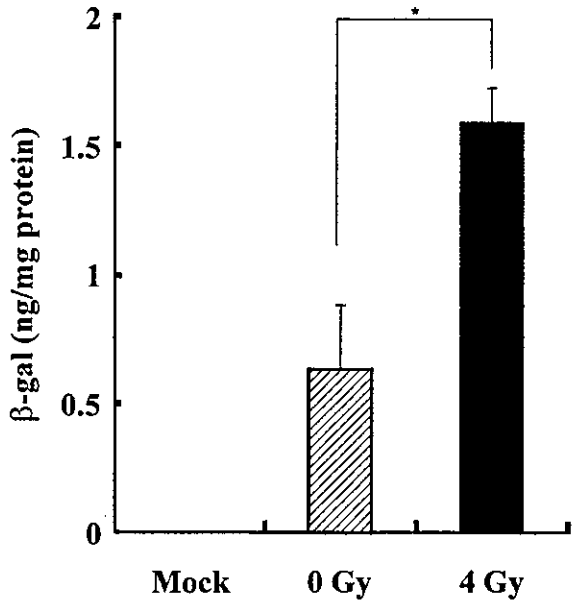

Figure 7 γ-Ray increased the expression level of β-galactosidase. The tumors were established by HEp-2 cells into the flanks of the mice xenografts. The tumors were injected with 5×10^{11} particles of AAVLacZ immediately after γ-ray irradiation at the dose of 0 or 4 Gy. Three days after AAVLacZ injection, the tumors were excised, homogenized, and assayed for the amount of β-galactosidase. Data were analyzed by one-way ANOVA. Asterisk means that the β-galactosidase expression level in 4 Gy irradiated tumors was significantly different from that in non-irradiated tumors ($P<0.01$). Each bar represents the mean ± s.d. ($n=3$).

half, and γ-ray irradiation augmented the antitumor activity five-fold as assessed by the relative tumor volume to the controls. The combined approach with AAVtk/GCV system and γ-ray irradiation suppressed the tumor growth for 30 days. These data were analyzed by two-way ANOVA ($P<0.01$).

Discussion

In this study, we demonstrated that γ-ray irradiation enhanced AAV vector-mediated transgene expression and cytocidal effect of AAVtk/GCV on target cells. These findings were also shown in animal experiments, ie γ-ray irradiation enhanced transgene expression and killing effect of the AAVtk/GCV upon the grafted tumors.

There is a possibility that the killing effect was contributed by HSVtk/GCV and γ-ray irradiation without AAV vectors. However, we made several experiments about the second-strand synthesis utilizing AAVLacZ and demonstrated that the enhanced killing effect can be explained by the higher conversion efficiency of AAV vector genome to double-stranded form. Although several studies have been reported on the higher conversion efficiency, the mechanism by which a genetic stress enhances the second-strand synthesis is not fully understood.[12–16] Qing *et al*[23] reported that dephosphorylation of the single-stranded D sequence-binding protein facilitated second-strand synthesis of the AAV vector genome. Sanlioglu *et al*[24] reported that the enhancement of AAV vector transduction by UV and adenovirus E4orf6 correlated with induction of two distinct molecular conversion pathways, and UV led to increased abundance of circular AAV vector genome. Some studies have shown that DNA repair synthesis is required for efficient transduction rather than replicative cellular DNA synthesis.[13,25] The machinery of cellular DNA repair synthesis may play an important role in converting the single-stranded AAV vector genome to a double-stranded form, which is activated by γ-ray irradiation.

Several studies reported that AAV vectors were useful for the treatment of cancers in model experiments. Kunke *et al*[3] showed that expressing the antisense of human papillomavirus early gene effectively killed the tumors derived from cervical cancer cells. Suicide gene therapy, in particular, HSVtk-expressing AAV vectors, was reported in the application to several kinds of cancers. The AAV vectors expressing HSVtk and interleukin 2 effectively killed glioma cells implanted into brains of nude mice.[26] The expression of HSVtk driven by a liver-specific promoter via AAV vectors in tumors experimentally produced by implantation of hepatocellular carcinoma cells successfully retarded the tumor progression.[27] We previously demonstrated the enhancement of the cytocidal effect of AAVtk/GCV system by

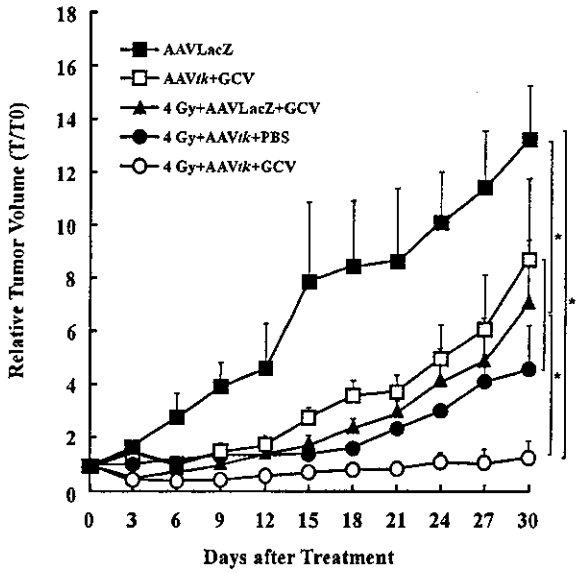

Figure 8 In vivo tumor growth inhibition with AAVtk/GCV treatment and γ-ray irradiation. The tumors derived from HEp-2 cells were established in the flanks of BALB/c nude mice by subcutaneous injection of the cell lines. Once established (a diameter of 4–5 mm), the tumors were irradiated at 4 Gy and then directly injected with 1×10^{12} particles of AAVLacZ or AAVtk. Administration of GCV (50 mg/kg) or PBS intraperitoneally twice a day was started 24 h after the virus injection and continued for 2 weeks. The tumors were measured every 3 days with calipers in two perpendicular diameters. Closed squares: AAVLacZ-injected animals (n=4); open squares: AAVtk-injected animals with GCV administration (n=5); closed triangles: AAVLacZ-injected animals with 4 Gy irradiation and GCV administration (n=5); closed circles: AAVtk-injected animals with 4 Gy irradiation and PBS administration (n=4); open circles: AAVtk-injected animals with 4 Gy irradiation and GCV administration. The relative tumor volume (T/T_0) was calculated as the ratio of tumor volumes at any time after the treatment (T) to that before the treatment (T_0). Data were analyzed by two-way ANOVA ($P<0.01$). Each data point represents the mean ± s.d.

γ-ray *in vitro*.[11] The AAVtk/GCV system effectively killed the cancer cells depending on the concentration of GCV. Moreover, when the cancer cells were irradiated prior to transduction with AAVtk, they were killed more efficiently in a dose-dependent manner.

To extend these *in vitro* findings to an animal model, in the present study, we investigated the enhancement of AAV-mediated transgene expression by γ-ray irradiation in nude mice. To confirm whether γ-ray enhances the transgene expression, the xenografted tumors were injected with AAVLacZ. γ-Ray irradiation increased the number of X-gal-positive cells and the amount of β-galactosidase as expected in the tumors *in vivo*. Furthermore, significantly higher growth inhibition of the xenografted tumors was observed in the 4 Gy irradiation plus AAVtk/GCV group compared with the AAVtk/GCV system alone, the 4 Gy irradiation plus AAVLacZ/GCV, or the AAVtk/PBS. The combination therapy using other vectors and irradiation has been reported,[21,22] but the augmentation of the second-strand synthesis by γ-ray irradiation is unique to AAV vectors.

Apoptosis induced by γ-ray irradiation enhances the bystander effects, which may allow nearby untransduced cells to take up the apoptotic vesicles containing phosphorylated toxic GCV metabolites.[21] Thus, the combination therapy of AAV-mediated suicide gene therapy with radiotherapy or other genotoxic stress such as chemotherapy seems to be valuable for the treatment of cancers.

Recently, the HSVtk mutants with improved GCV-mediated killing and bystander effect have been developed.[28–30] Since GCV has side effects such as pancytopenia[31] and acute renal failure,[32] the concentration of GCV should be kept as low as possible. In this study, the concentration of GCV was higher than the standard experiments, this concentration was chosen because the difference in the killing effects was most prominent among the groups, and the animals well tolerated throughout the study.

Our model would be another alternative to improve AAV-mediated suicide gene therapy of cancer. Although several studies were reported on combining radiotherapy and viral vector mediated gene therapy,[22,33] our therapeutic model made it with lower dose of irradiation. AAV-mediated suicide gene therapy and γ-ray irradiation may provide a more effective and safer alternative for the treatment of head and neck cancer.

Materials and methods

Cell lines

To compare the transgene expression between head and neck cancer cells and the cells used in the standard experiments, we used HeLa cells other than the head and neck cancer cells. HeLa cells and a human laryngeal carcinoma cell line, HEp-2 cells (a gift from the Cell Resource Center for Biomedical Research, Tohoku University), were cultured in DMEM/F12 (Gibco-BRL, Grand Island, NY, USA) supplemented with 10% heat-inactivated fetal bovine serum, 100 U/ml of penicillin and 100 μg/ml of streptomycin (Irvine Scientific, Santa Ana, CA, USA) at 37°C in 5% CO_2.

Plasmids

The plasmid pAAVLacZ contains the cytomegalovirus (CMV) promoter, human growth hormone first intron, *E. coli* LacZ gene, and SV40 early polyadenylation sequence between two inverted terminal repeats. A 1.8 kb DNA fragment encoding the HSVtk gene was obtained by double digestion with *Hinc* II and *Pvu* II of plasmid M2[34] (a gift from Dr Y Mishina, Yokohama City University, Japan) and subcloned into the pAAVLacZ in the place of the LacZ gene (pAAVtk). pW1909 is an AAV helper plasmid harboring rep/cap sequences, in which the p5 promoter was moved to downstream of the poly A signal to enhance AAV vector production.[35] An adenovirus helper plasmid plAd5 contains the adenovirus early genes: E2a, E4, and VA.[36]

AAV vector production

AAV vectors were produced based on the plasmid transfection.[36] Briefly, subconfluent 293 cells were co-transfected with AAV vector plasmid, pW1909, and adenovirus helper plasmid by a calcium phosphate precipitation method. Recombinant AAV was harvested by three cycles of freeze/thaw. The vector solution was then purified twice on a CsCl gradient as described previously.[36] The vector titer was determined by a quantitative dot blot hybridization of DNase-treated stocks.

Transduction of HeLa or HEp-2 cells with AAV vectors

One day before transduction, 1×10^5 cells were plated onto 3.5 cm dishes in triplicate. The cells were transduced with different amounts of AAVLacZ.

Assay for β-galactosidase activity

Thirty-six hours after transduction with AAVLacZ, the cells were fixed by 0.05% glutaraldehyde in PBS and stained with X-gal (Takara, Tokyo, Japan) in PBS containing 5 mM $K_3[Fe(CN)_6]$, 5 mM $K_4[Fe(CN)_6]$, and 1 mM $MgCl_2$.[37] For each dish, 500 cells were counted by light microscopy and the percentage of blue stained cells was determined. An average of three wells was determined for each variable. In addition, the amount of β-galactosidase was quantified by using the β-gal ELISA kit (Boehringer-Mannheim, Hilden, Germany).

The enhancement of transgene expression by γ-ray irradiation

To examine whether γ-ray enhances the transgene expression in HeLa and HEp-2 cells, the cells were plated at a density of 1×10^5 cells/well in six-well culture plates 24 h prior to irradiation at doses of 0–5 Gy. Irradiation was done using GAMMACELL-40 (Atomic Energy of Canada, Ottawa, Canada) at a dose rate of 0.83 Gy/min. The cells were then transduced with 1×10^3 particles/cell of AAVLacZ immediately after irradiation. Thirty-six hours after transduction, we measured the amount of β-galactosidase with the β-gal ELISA.

Analysis of the second-strand synthesis of the vector genome

HeLa and HEp-2 cells grown in 10 cm dishes (1×10^6/dish) were transduced with 1×10^4 particles/cell of AAVLacZ immediately after irradiation. Two days later, total DNA was isolated under a low-salt condition (10 mM Tris–HCl [pH 7.5], 5mM EDTA, and 0.5% sodium dodecyl sulfate) to prevent annealing of the AAVLacZ genomes.[38] Forty micrograms of genomic DNA digested with 80 units of mung bean nuclease (Takara, Tokyo, Japan) was resolved on 1% agarose gels, transferred to nylon membranes (Hybond N^+; Amersham, Buckinghamshire, UK) and then hybridized with CMV promoter-specific probe radiolabeled with random primer labeling kit (Amersham, Buckinghamshire, UK) in 50% formamide, 6 × SSC, 0.5% SDS, 5 × Denhardt's solution, and 100 μg/ml of denatured salmon sperm DNA at 42°C overnight. The membranes were washed, and then analyzed by using an image analyzer (BAS-1500, Fuji, Tokyo, Japan).

GCV treatment

The cells were plated and transduced with AAVtk at the dose of 1×10^5 particles/cell. Twenty-four hours after transduction with AAV vectors, culture media were replaced by fresh media containing various concentrations of GCV ranging from 0 to 10 μg/ml. After a 7-day incubation in the presence of GCV, surviving cells were counted. The survival rate was calculated from the ratio of the number of surviving cells to the number of cells not treated with GCV. To evaluate the synergistic effect of the AAVtk/GCV system and γ-ray irradiation, the cells were irradiated at doses of 2 or 4 Gy just before AAV vector transduction.

Animal experiments

Female BALB/c nude mice (between 4 and 5 weeks of age) were purchased from CLEA Japan, Inc. (Tokyo, Japan) and maintained in the specific pathogen-free animal facility at Jichi Medical School. The HEp-2 cells (2×10^6/mouse) with 25% Matrigel (Collaborative Research, Bedford, MA, USA) were injected subcutaneously into the flanks of the mice. The tumors were irradiated by the GAMMACELL-40.

Assay for β-galactosidase in tumors

To examine whether γ-rays enhance the transgene expression *in vivo*, 5×10^{11} particles of AAVLacZ were injected into the tumors in a diameter of 4–5 mm immediately after 4 Gy irradiation. Three days after AAVLacZ was injected, the tumors were excised from mice and frozen in OTC embedding compound on a liquid-nitrogen bath. Cryostat sections (20 μm thick) were made with a Cryotome CR-502 (Nakagawa, Tokyo, Japan) and were fixed with 0.05% glutaraldehyde in PBS. Histochemical staining for β-galactosidase activity was performed in the sections, as described above and counterstained with nuclear fast red. Furthermore, to quantify the amount of β-galactosidase in the non-irradiated or 4 Gy irradiated tumor, these samples were homogenized for 10 s in a tissue homogenizer. The homogenates were centrifuged twice and aliquots of the supernatants were prepared for the assay with β-gal ELISA kit (Boehringer-Mannheim). Four mice were used in each treatment group.

In vivo gene therapy

To examine the tumor growth inhibition, 1×10^{12} particles of AAVtk or AAVLacZ as control were injected into the tumors immediately after 4 Gy irradiation. Administration of GCV (50 mg/kg) or PBS intraperitoneally twice a day was started 24 h after the virus infection and continued for 2 weeks. The tumors were measured every 3 days with calipers in two perpendicular diameters. The tumor volume was calculated as $0.5 \times L \times W^2$, where L is the length (mm) and W is the width (mm).[39] The tumors reaching a diameter of 4–5 mm were used as the starting point for the study of tumor growth or regression.

Acknowledgements

We thank Dr M Nakazawa (Department of Radiology, Jichi Medical School) for technical advice and helpful discussion. We also thank Avigen Inc., for providing the plasmids, pAAVLacZ, pW1909 and plAd, and the Cell Resource Center for Biomedical Research, Tohoku University for providing the HEp-2 cells.

This work was supported in part by grants from the Ministry of Health, Labor and Welfare of Japan, Grants-in-Aid for Science Research from the Ministry of Education, Culture, Sports, Science and Technology of Japan, CREST (Core Research for Evolutional Science and Technology), and Special Coordination Funds for promoting Science and Technology of the Science and Technology Agency of Japanese Government.

References

1 Merino OR, Lindberg RD, Fletcher GH. An analysis of distant metastases from squamous cell carcinoma of the upper respiratory and digestive tracts. *Cancer* 1977; **40**: 145–151.

2 Clayman GL *et al*. *In vivo* molecular therapy with p53 adenovirus for microscopic residual head and neck squamous carcinoma. *Cancer Res* 1995; **55**: 1–6.

3 Kunke D *et al*. Preclinical study on gene therapy of cervical carcinoma using adeno-associated virus vectors. *Cancer Gene Ther* 2000; **7**: 766–777.

4 Su H, Lu R, Ding R, Kan YW. Adeno-associated viral-mediated gene transfer to hepatoma: thymidine kinase/interleukin 2 is more effective in tumor killing in non-ganciclovir (GCV)-treated than in GCV-treated animals. *Mol Ther* 2000; **1**: 509–515.

5 Berns KI, Rose JA. Evidence for a single-stranded adenovirus-associated virus genome: isolation and separation of complementary single strands. *J Virol* 1970; **5**: 693–699.

6 Blacklow NR *et al*. A seroepidemiologic study of adenovirus-associated virus infection in infants and children. *Am J Epidemiol* 1971; **94**: 359–366.

7 Muzyczka N. Use of adeno-associated virus as a general transduction vector for mammalian cells. *Curr Top Microbiol Immunol* 1992; **158**: 97–129.

8 Wagner JA *et al*. Efficient and persistent gene transfer of AAV-CFTR in maxillary sinus. *Lancet* 1998; **351**: 1702–1703.

9 Muramatsu S *et al*. Behavioral recovery in a primate model of Parkinson's disease by triple transduction of striatal cells with adeno-associated viral vectors expressing dopamine-synthesizing enzymes. *Hum Gene Ther* 2002; **13**: 345–54.

10 Kay MA *et al*. Evidence for gene transfer and expression of factor IX in haemophilia B patients treated with an AAV vector. *Nat Genet* 2000; **24**: 257–261.

11 Kanazawa T *et al*. Gamma-rays enhance rAAV-mediated transgene expression and cytocidal effect of AAV-HSVtk/ganciclovir on cancer cells. *Cancer Gene Ther* 2001; **8**: 99–106.

12 Ferrari FK, Samulski T, Shenk T, Samulski RJ. Second-strand synthesis is a rate-limiting step for efficient transduction by recombinant adeno-associated virus vectors. *J Virol* 1996; **70**: 3227–3234.

13 Fisher KJ *et al*. Transduction with recombinant adeno-associated virus for gene therapy is limited by leading-strand synthesis. *J Virol* 1996; **70**: 520–532.

14 Alexander IE, Russell DW, Miller AD. DNA-damaging agents greatly increase the transduction of nondividing cells by adeno-associated virus vectors. *J Virol* 1994; **68**: 8282–8287.

15 Alexander IE, Russell DW, Spence AM, Miller AD. Effects of gamma irradiation on the transduction of dividing and nondividing cells in brain and muscle of rats by adeno-associated virus vectors. *Hum Gene Ther* 1996; **7**: 841–850.

16 Peng D *et al*. Transduction of hepatocellular carcinoma (HCC) using recombinant adeno-associated virus (rAAV): *in vitro* and *in vivo* effects of genotoxic agents. *J Hepatol* 2000; **32**: 975–985.

17 Trask TW *et al*. Phase I study of adenoviral delivery of the HSV-tk gene and ganciclovir administration in patients with current malignant brain tumors. *Mol Ther* 2000; **1**: 195–203.

18 Hasenburg A *et al*. Thymidine kinase gene therapy with concomitant topotecan chemotherapy for recurrent ovarian cancer. *Cancer Gene Ther* 2000; **7**: 839–844.

19 Sutton MA *et al*. *In vivo* adenovirus-mediated suicide gene therapy of orthotopic bladder cancer. *Mol Ther* 2000; **2**: 211–217.

20 Makinen K *et al*. Evaluation of herpes simplex thymidine kinase mediated gene therapy in experimental pancreatic cancer. *J Gene Med* 2000; **2**: 361–367.

21 Kawashita Y *et al*. Regression of hepatocellular carcinoma *in vitro* and *in vivo* by radiosensitizing suicide gene therapy under the inducible and spatial control of radiation. *Hum Gene Ther* 1999; **10**: 1509–1519.

22 Rogulski KR *et al*. Double suicide gene therapy augments the antitumor activity of a replication-competent lytic adenovirus through enhanced cytotoxicity and radiosensitization. *Hum Gene Ther* 2000; **11**: 67–76.

23 Qing K *et al*. Adeno-associated virus type 2-mediated gene transfer: correlation of tyrosine phosphorylation of the cellular single-stranded D sequence-binding protein with transgene expression in human cells *in vitro* and murine tissues *in vivo*. *J Virol* 1998; **72**: 1593–1599.

24 Sanlioglu S, Duan D, Engelhardt JF. Two independent molecular pathways for recombinant adeno-associated virus genome conversion occur after UV-C and E4orf6 augmentation of transduction. *Hum Gene Ther* 1999; **10**: 591–602.

25 Russell DW, Alexander IE, Miller AD. DNA synthesis and topoisomerase inhibitors increase transduction by adeno-associated virus vectors. *Proc Natl Acad Sci USA* 1995; **92**: 5719–5723.

26 Okada H *et al*. Gene therapy against an experimental glioma using adeno-associated virus vectors. *Gene Ther* 1996; **3**: 957–964.

27 Su H, Lu R, Chang JC, Tissue-specific expression of herpes simplex virus thymidine kinase gene delivered by adeno-associated virus inhibits the growth of human hepatocellular carcinoma in athymic mice. *Proc Natl Acad Sci USA* 1997; **94**: 13 891–13 896.

28 Qiao J, Black ME, Caruso M. Enhanced ganciclovir killing and bystander effect of human tumor cells transduced with a retroviral vector carrying a herpes simplex virus thymidine kinase gene mutant. *Hum Gene Ther* 2000; **11**: 1569–1576.

29 Howard BD *et al*. Transduction of human pancreatic tumor cells with vesicular stomatitis virus G-pseudotyped retroviral vectors containing a herpes simplex virus thymidine kinase mutant gene enhances bystander effects and sensitivity to ganciclovir. *Cancer Gene Ther* 2000; **7**: 927–938.

30 Valerie K *et al*. Improved radiosensitization of rat glioma cells with adenovirus-expressed mutant herpes simplex virus-thymidine kinase in combination with acyclovir. *Cancer Gene Ther* 2000; **7**: 879–884.

31 Buhles WC *et al*. Ganciclovir treatment of life- or sight-threatening cytomegalovirus infection: experience in 314 immunocompromised patients. *Rev Infect Dis* 1988; **10**: S495–S506.

32 Snydman DR. Ganciclovir therapy for cytomegalovirus disease associated with renal transplants. *Rev Infect Dis* 1988; **10**: S554–S562.

33 Hanna NN *et al*. Virally directed cytosine deaminase/5-fluorocytosine gene therapy enhances radiation response in human cancer xenografts. *Cancer Res* 1997; **57**: 4205–4209.

34 Wilkie NM *et al*. Hybrid plasmids containing an active thymidine kinase gene of Herpes simplex virus 1. *Nucleic Acids Res* 1979; **7**: 859–877.

35 Ogasawara Y *et al*. Efficient production of adeno-associated virus vectors using split-type helper plasmids. *Jpn J Cancer Res* 1999; **90**: 476–483.

36 Matsushita T *et al*. Adeno-associated virus vectors can be efficiently produced without helper virus. *Gene Ther* 1998; **5**: 938–945.

37 Cepko C. Preparation of a specific retrovirus producer cell line. In: Ausubel FM, Brent R, Kingston RE, Moore DD, Seidman JG, Smith JA, Struhl K (eds). *Current Protocols in Molecular Biology*. John Wiley & Sons: New York, 1995, pp 9.10.1–9.10.13.

38 Ozawa K, Kurtzman G, Young N. Replication of the B19 parvovirus in human bone marrow cell cultures. *Science* 1986; **233**: 883–886.

39 Kung AL *et al*. Suppression of tumor growth through disruption of hypoxia-inducible transcription. *Nat Med* 2000; **6**: 1335–1340.

The Laryngoscope
Lippincott Williams & Wilkins, Inc.
© 2003 The American Laryngological,
Rhinological and Otological Society, Inc.

Temporal Bone Histopathological and Quantitative Analysis of Mitochondrial DNA in MELAS

Katsumasa Takahashi, MD; Saumil N. Merchant, MD; Tetsuo Miyazawa, MD; Toshikazu Yamaguchi, PhD; Michael J. McKenna, MD; Hiroko Kouda, MD; Yukiko Iino, MD; Tsutomu Someya, MD; Yuya Tamagawa, MD; Yoshihisa Takiyama, MD; Imaharu Nakano, MD; Ken Saito, MD; Philip Boyer, MD, PhD; Ken Kitamura, MD

Objectives/Hypothesis: **Although hearing loss is common in MELAS (syndrome of mitochondrial encephalopathy, lactic acidosis and stroke-like episodes), the histopathology of the temporal bone has not been reported. The majority of cases of MELAS are linked to a mitochondrial DNA (mtDNA) mutation at nucleotide 3243. In MELAS, normal mtDNA and mutant mtDNA coexist in a heteroplasmic manner. The purpose of the study was to report the otopathological findings from two patients with MELAS and quantitative mtDNA analysis in the inner ear of one of these patients.** ***Study Design:*** **Basic scientific histopathological examination and quantitative mtDNA analysis of the temporal bone.** ***Methods:*** **Temporal bones were embedded in celloidin and sectioned for light microscopic study. Graphic reconstruction of the cochlea was performed using the method described by Schuknecht. For quantitative mtDNA analysis, total DNA from the membranous part of the inner ear was collected, amplified by polymerase chain reaction, and digested with the restriction enzyme. The percentage of mutant/total mtDNA was measured by the ratio of fluorescence intensity.** ***Results:*** **Histopathological examination revealed severe degeneration of the stria vascularis and degenerative change of spiral ganglion cells in both patients. The quantitative DNA studies showed that the proportion of mutant to wild-type mtDNA was similar in both histologically affected and histologically unaffected tissues within the inner ear.** ***Conclusion:*** **Dysfunction of the stria vascularis and spiral ganglion cells causes sensorineural hearing loss in MELAS.** ***Key Words:*** **Mitochondrial DNA, MELAS, hearing loss, histopathology, heteroplasmy.**

Laryngoscope, **113:1362–1368, 2003**

INTRODUCTION

A mutation of the mitochondrial transfer RNA (tRNA) Leu gene (3243 A to G) is linked to MELAS (syndrome of mitochondrial encephalopathy, lactic acidosis, and stroke-like episodes),[1,2] and 30% to 70% of patients with MELAS have sensorineural hearing loss (SNHL).[3–6] Clinical studies have suggested that the SNHL is often bilateral, generally symmetrical and progressive, with a downsloping or flat audiometric pattern. Asymmetrical SNHL with stepwise progression has also been reported. Speech discrimination scores are variable, being preserved in some patients with SNHL and poor in others, out of proportion to the degree of hearing loss. Furthermore, auditory evoked brainstem response (ABR) and otoacoustic emission testing has suggested both cochlear and retrocochlear involvement in hearing loss due to MELAS.[4,5] The histopathology of the inner ear in MELAS has not been previously reported. In MELAS, the mutant mitochondrial DNA (mtDNA) at nucleotide 3243 coexists with normal mtDNA in a heteroplasmic manner, so the distribution of mutant mtDNA varies in different tissues. Although the mutant-to-normal mtDNA ratio of various tissues has been reported,[7–9] the ratio within the inner ear has not been studied. In the present study, we report

Presented at the Conference on The Molecular Biology of Hearing and Deafness, Bethesda, MD, October 8–11, 1998.

From the Department of Otolaryngology (K.T.), Gunma University, Maebashi, Gunma, Japan; the Departments of Otolaryngology (YU.T.), Neurology (YO.T, I.N.), and Pathology (T.S., K.S.), Jichi Medical School, Minamikawachi, Tochigi, Japan; the Department of Otolaryngology (S.N.M, M.J.M.), Massachusetts Eye and Ear Infirmary, Harvard Medical School, Boston, Massachusetts, U.S.A.; the Department of Otolaryngology (T.M., Y.I.), Teikyo University, Itabashi-ku, and the Department of Otolaryngology (H.K., K.K.), Tokyo Medical and Dental University, Bunkyo-ku, Tokyo, Japan; BML General Laboratory (T.Y.), Kawagoe, Saitama, Japan; and the Department of Pathology (P.B.), Pennsylvania State University, Hershey, Pennsylvania, U.S.A.

Supported in part by a Grant-in-Aid for Science Research (grant 11470358) from the Ministry of Science, Education, Sports and Culture of Japan; a Health Sciences Research Grant (Research on Eye and Ear Science, Immunology, Allergy, and Organ Transplantation) from the Ministry of Health and Welfare of Japan; and grant 5 RO1 DC03401 from the National Institute on Deafness and Other Communication Disorders, National Institutes of Health, Bethesda, MD.

Editor's Note: This Manuscript was accepted for publication May 7, 2003.

Send Correspondence to Ken Kitamura, MD, Department of Otolaryngology, Tokyo Medical and Dental University, Bunkyo-ku, Tokyo 113-8519, Japan. E-mail address: kitamura.oto@tmd.ac.jp

the otopathological findings from two cases with MELAS and a quantitative analysis of mutant mtDNA in the inner ear of one of these cases.

CASE REPORTS

Case 1

In case 1, the patient was asymptomatic in her childhood. She had her first episode of convulsions at age 14 years followed by frequent episodes of vomiting with headache. On hospitalization at age 17, she was noted to have intellectual deterioration and bilateral, symmetrical, downsloping SNHL with speech discrimination scores of 58% in the right ear and 54% in the left ear (Fig. 1A). She also complained of tinnitus, vertigo, loss of appetite, and poor vision. Serum pyruvate and lactate levels were both elevated. Ragged red fibers were observed in a muscle biopsy specimen. A clinical diagnosis of MELAS was made, and blood DNA testing revealed the typical mtDNA 3243 A to G mutation. She had repeated convulsive episodes and developed hemiplegia. Intellectual deterioration and SNHL progressed gradually. An ABR test at age 17 years revealed presence of all waves from I to V in each ear, whereas an ABR test at age 22 showed only a poorly formed wave V in each ear (at 100 dB) with a delayed latency of 6.0 milliseconds. The Metz test result was positive, indicating the presence of recruitment.[10] Her last audiogram was at age 27 years (Fig. 1A), which showed a bilateral, symmetrical, generally flat SNHL of approximately 60 dB. Speech discrimination testing was not performed at that time because of her cognitive problems. Electronystagmography was performed at age 21 years. On caloric testing with 10 mL ice water, the maximal slow phase of the caloric nystagmus was 9.4°/s in the right ear and 8.8°/s in the left ear, which was consistent with decreased vestibular function in both ears. Optokinetic nystagmus was poorly elicited, and an ataxic pursuit eye movement was recorded in the eye tracking test, which suggested a central lesion in the cerebellum and/or brainstem. Posturography and stepping test confirmed her severe disequilibrium. She received a diagnosis of severe diabetes mellitus at age 22 years. At age 30, she had pneumonia and her general condition deteriorated. She died of multisystem organ failure at 30 years of age. No facial palsy was noted during her entire life. Her mother, who also has MELAS, is still alive, whereas her younger sister died in childhood of convulsions of unknown cause. There were no other family members affected with MELAS. The patient's MELAS was inherited from her mother.

Case 2

In case 2, the patient became symptomatic at age 10 years, when she had her first seizure. At age 11, she developed a bilateral, downsloping, high-frequency, symmetrical SNHL with speech discrimination scores of 88% in both ears. The SNHL was progressive, and she was fitted with binaural amplification. An ABR test at age 14 years revealed only waves I and V in each ear but did not indicate retrocochlear disease. Another ABR test at age 16 showed only a poorly formed wave V in each ear (at 120 dB) with a delayed latency of 6.5 milliseconds. Audiometric evaluation at age 16 revealed a symmetrical, bilateral, downsloping 25- to 90-dB SNHL with speech discrimination scores of 64% in both ears. Another evaluation a year later, at age 17 years, showed similar pure-tone thresholds, but speech discrimination was not tested (Fig. 2). A final audiological evaluation was performed at age 19 years; the patient was too ill to provide reliable or consistent responses to pure tones. However, using speech as a stimulus, her hearing was estimated to be in the 40- to 60-dB range. Multiple organ systems were affected, resulting in seizures, multiple strokes, gastrointestinal dysmotility, urinary incontinence and multiple urinary tract infections, diabetes, anemia, lactic acidosis, generalized myopathy, and multiple respiratory tract infections. A diagnosis of MELAS was made based on a positive muscle biopsy specimen that showed ragged red fibers, elevated lactic acids in blood with elevated lactate-to-pyruvate ratio, and blood DNA testing that revealed the mtDNA 3243 A to G mutation. She died of multisystem organ failure at age 23 years. The patient's mother, who is still alive, has hearing

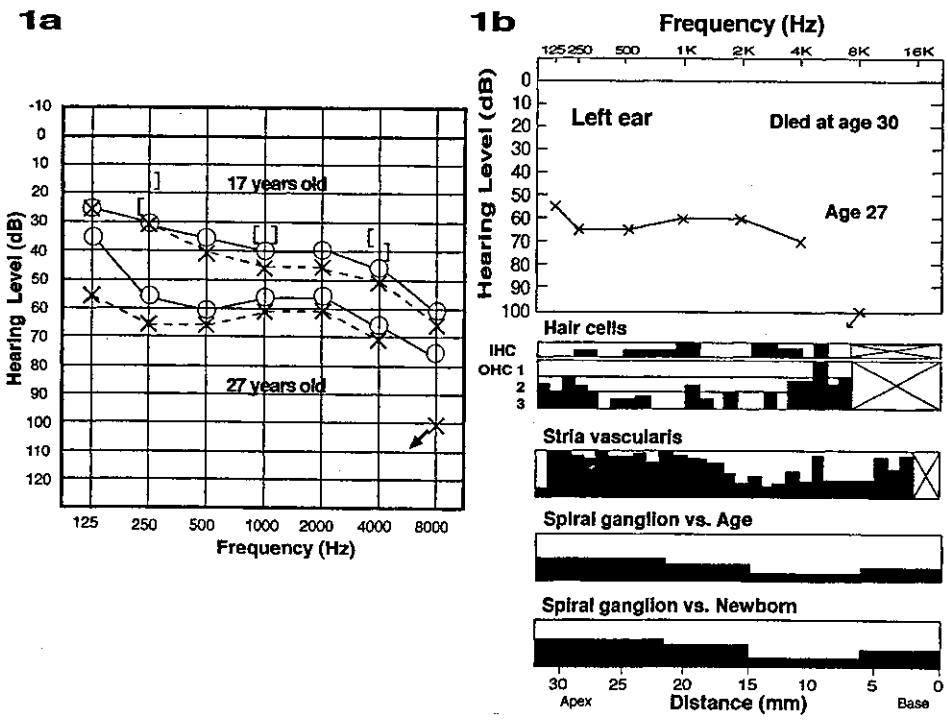

Fig. 1. Audiograms and cytocochleogram of patient in case 1. (A) Pure-tone audiograms at ages 17 and 27 years, showing a progressive, bilateral and symmetrical sensorineural hearing loss. Speech discrimination scores were 58% in the right ear and 54% in the left ear at age 17 years; speech discrimination was not tested at age 27. (B) Audiogram and cytocochleogram of left ear. Graphic reconstruction of the cochlea (cytocochleogram) was performed according to the method described by Schuknecht.[11] The black areas in the cytocochleogram represent missing or abnormal elements. The inner and outer hair cells are shown as present (white) or absent (black). Vertical axis of the cytocochleogram for the stria and neurons represents percentage of loss. Areas within the hair cell histograms marked by "X" represent regions where cytological evaluations could not be performed. There was severe atrophy of the stria vascularis, especially in the apical half of the cochlea. There were partial losses of outer and inner hair cells (OHC and IHC, respectively). There was moderate loss of spiral ganglion cells (neurons) when compared with mean counts from age-matched control samples or newborns.

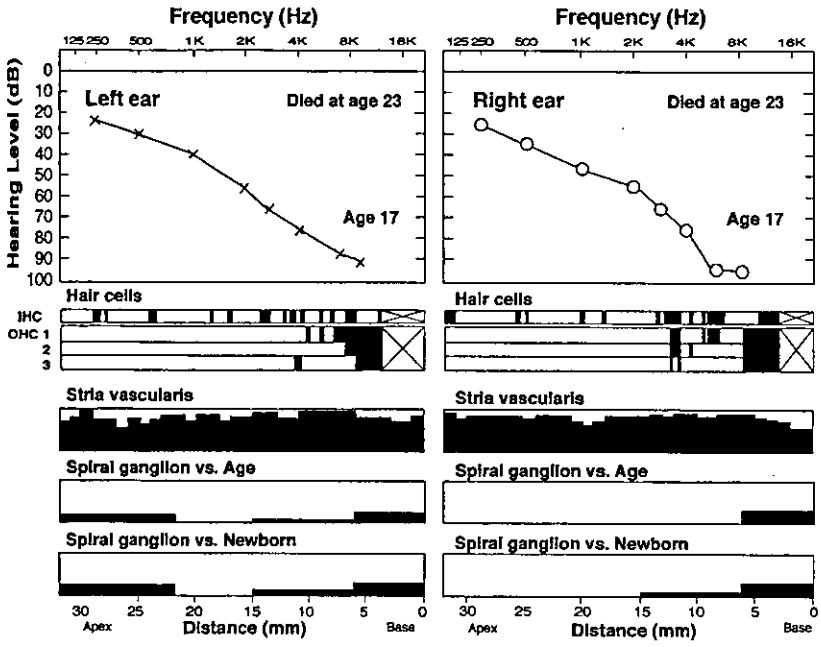

Fig. 2. Audiogram and cytocochleograms of patient in case 2. The audiogram at age 17 years showed a bilateral, downsloping, symmetrical sensorineural hearing loss. Speech discrimination testing was not performed. However, audiological evaluation 1 year earlier, at age 16 years, had revealed similar pure-tone thresholds and 64% speech discrimination in each ear. Graphic reconstruction of the cochlea (cytocochleogram) was performed in the same way as in Fig. 1. The diffuse, severe atrophy of the stria vascularis is evident in all turns. Both outer and inner hair cells (OHC and IHC, respectively) were generally present. There was a mild loss of the spiral ganglion cells (neurons) when compared with mean counts from newborns or age-matched control samples.

loss, diabetes, and visual loss. The patient's maternal uncle also has hearing loss. The family history is consistent with maternal inheritance of mitochondrial disease in this patient.

MATERIALS AND METHODS

Histological Study

Temporal bones were harvested 3 hours postmortem in case 1 and 7 hours postmortem in case 2. All bones, except the right ear in case 1, were fixed by 10% neutral buffered formaldehyde, decalcified by EDTA, dehydrated by a series of alcohols of increasing concentration, and embedded in celloidin. Sections were cut at a thickness of 20 μm. Every tenth section was double-stained with H&E and examined by light microscopy. Graphic reconstruction of the cochlea was performed using the method described by Schuknecht[11] to determine loss of various neurosensory elements including hair cells, stria vascularis, and spiral ganglion cells. Hair cells were recorded as being present or absent. Atrophy of the stria vascularis was estimated as a percentage of normal. The number of spiral ganglion cells was counted and was expressed as a percentage of normal for age-matched control subjects and newborns.[11] These quantitative data were used to create cytocochleograms. Scarpa ganglion cell counts were also performed in case 2 and compared with normative data.[12] The brainstems in both cases were fixed in 10% neutral buffered formalin, embedded in paraffin, and sectioned at 6 μm, followed by staining with H&E and Luxol fast blue H&E for light microscopic study.

Quantitative Analysis of Mutant Mitochondrial DNA

Quantitative analysis of mutant mtDNA was performed on the right ear in case 1. The specimen was fixed by 10% neutral buffered formaldehyde and decalcified by EDTA. The membranous part of the inner ear was dissected under the microscope, and the following samples were obtained: 1) the organ of Corti, 2) stria vascularis, 3) lateral semicircular canal, and 4) facial nerve. The samples were digested using 600 μg/mL proteinase K (TaKaRa, Shiga, Japan) for a day at 37°C. Total DNA was obtained by En-Zap kit (Bio Ventures, Inc., Murfreesboro, TN) and rehydrated by TE solution (10 mmol/L Tris-HCl and 10 mmol/L EDTA). Several organs, including occipital lobe of the brain, pancreas, quadriceps skeletal muscle, and spleen, were obtained at autopsy and stored immediately at −80°C. The DNA of these organs was extracted by phenol and chloroform, precipitated by alcohol, dried, and rehydrated by TE solution. DNA from leukocytes had been previously extracted during life. DNA of leukocytes from a healthy man was used as a negative control. To quantify the ratio of mutant-to-total mtDNA (expressed as a percentage), we used the method described by Yu et al.[13] The mtDNA was amplified using polymerase chain reaction (PCR), a sense primer 5'-TCATCTCAACTTAGTATTAT-3' (3183–3202), and an antisense primer 5'-rhodamine-GTTAAGAAGAGGAATGAACC-3' (3283–3303). The antisense primer was labeled by rhodamine for quantitative analysis. The method for PCR thermocycling included 1) initial denaturation at 94°C for 3 minutes, 2) denaturation at 94°C for 30 seconds, 3) annealing at 45°C for 30 seconds, 4) extension at 72°C for 1 minute, 5) 27 repetitions of steps 2–4, and 6) final extension at 72°C for 7 minutes. The amplified mtDNA fragments were digested with the restriction enzyme Apa I (TaKaRa) at 37°C for 6 hours. The digested product was separated by 4% polyacrylamide gel electrophoresis, and each product was quantified by a fluorescence analyzer FMBIO 100 (Hitachi Software Engineering, Tokyo, Japan). The percentage of mutant/total mtDNA was measured by the ratio of fluorescent intensity of the mutant fragment. The PCR product from normal mtDNA was resistant to Apa I digestion, whereas a mutation with A to G transition generated an Apa I site in the mutant mtDNA and its PCR product was cleaved into two fragments. The antisense primer was labeled by fluorescence (rhodamine) so that normal mtDNA was detected as a long band (121 base pairs [bp]), whereas mutant mtDNA was detected as a short band (59 bp) on gel electrophoresis. The standard curve was measured so that the fluorescent intensity of the mutant fragment could be expressed as a percentile.[13]

RESULTS

Temporal Bone Histopathology

Case 1 (Left Ear) The most characteristic histological finding was marked atrophy of the stria vascularis,

especially in the apical half of the cochlea (Figs. 1B and 3A). An accumulation of round cells was present in the remaining stria (Fig. 3E). The organ of Corti showed partial losses of inner and outer hair cells (Fig. 1B). Moderate loss of spiral ganglion cells was observed in all turns of the cochlea (Figs. 1B and 3D). The total spiral ganglion count was 20,025, representing a 36% loss when compared with age-matched control samples and a 43% loss when compared with counts from normal newborns.[11] There was pathological collapse of the membranous wall of the saccule, as well as a significant hair cell loss in the saccular macula (Fig. 3F). The cristae of all three semicircular canals and the utricular maculae showed reduced numbers of hair cells. Dark cells appeared to be normal. Blood vessels supplying the inner ear appeared to be normal. There was no endolymphatic hydrops or collapse of Reissner's membrane. The endolymphatic duct and sac were of normal size. The vestibular nerve in the cribrose area was normal. Scarpa ganglion cells were not studied because the vestibular nerve trunk was avulsed from the temporal bone specimen. The facial nerve and the geniculate ganglion cells appeared normal. The audiogram and cytocochleogram of the left ear are presented in Fig. 1B. Light microscopic examination of the brainstem showed marked loss of neuronal cells within both ventral cochlear nuclei, with severe gliosis (Fig. 3C). In contrast, the remainder of the auditory pathway, including the superior olives, the inferior colliculi, and associated tracts including the trapezoid body and the lateral lemniscus, as well as the vestibular nuclei, appeared normal (data not shown). Quantitative measurements (such as cell number or volume) of neurons in the central pathways were not performed.

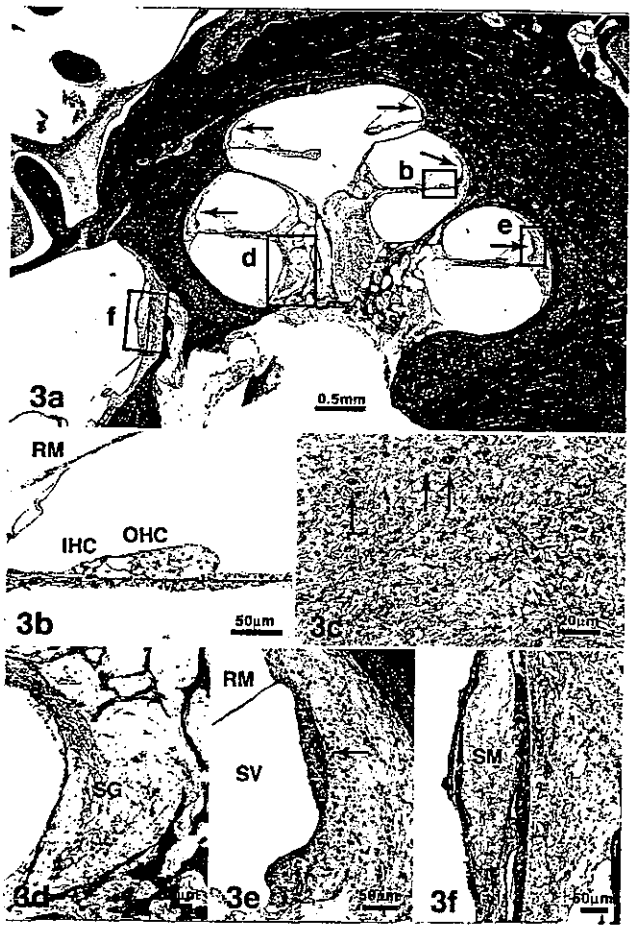

Fig. 3. Histopathological appearance of the left temporal bone of patient in case 1. (A) Mid-modiolar section of the cochlea. Diffuse, severe atrophy of the stria vascularis is evident in all turns (arrows). (B) Inner and outer hair cells (IHC and OHC, respectively) were present in the middle turn. (C) High-power view of the ventral cochlear nucleus showed loss of neurons and prominent gliosis. Only a few neurons are evident (arrows). (D) A high-power view of Rosenthal's canal demonstrated loss of spiral ganglion cells (SG). (E) High-power view of the stria vascularis (SV) in the basal turn showed partial atrophy and accumulation of round cells (arrow). Reissner's membrane (RM) is visible. (F) High-power view of the saccular macula (SM) showing collapsed saccular membrane and loss of hair cells.

Case 2 (Both Ears)

Both inner ears were similar. The audiogram and cytocochleogram of both ears are shown in Figure 2. The most notable change in the cochleae was diffuse, severe atrophy of the stria vascularis in all turns (Figs. 2 and 4). The few remaining strial cells showed vacuole formation and the presence of small, dark-staining, round and ovoid cells (Fig. 4B). Both outer and inner hair cells were generally present with scattered losses in the lower basal turns (Figs. 2 and 4B). The total spiral ganglion counts were 28,719 in the right ear and 32,742 in the left, representing a mild neuronal loss when compared with mean values of normal newborn and age-matched control samples (Fig. 2).[11] Many spiral ganglion cells showed varying degrees of degenerative change as evidenced by faint staining of the cytoplasm, loss of cell membrane outline, and loss of nuclear definition. There was no endolymphatic hydrops or collapse of Reissner's membrane. The cristae and maculae showed reduced numbers of hair cells compared with age-matched control samples. Dark cells were present in the vestibular organs. Scarpa ganglion cell counts were 13,543 on the right side and 14,564 on the left. Thus, the numbers of Scarpa ganglion cells were reduced to approximately 70% of mean counts of age-matched control samples.[12] The geniculate ganglion cells did not show degenerative changes of the type that were observed in the cochlear neurons. Light microscopic examination of the brainstem showed that the vestibular and cochlear nuclei, superior olives, the inferior colliculi and associated tracts, including the trapezoid body and the lateral lemniscus, were present. Quantitative measurement (such as cell density or volume) of neurons in the central pathways was not performed. The central neuropathological findings in case 2 have been previously reported.[14]

Content of Mutant Mitochondrial DNA in Inner Ear and Related Tissues

In case 1, long bands (normal mtDNA) and short bands (mutant mtDNA) were detected in various concentrations (Fig. 5, lanes 1–9), whereas no mutant mtDNA band was seen in the lane from the normal subject (Fig. 5, lane 10). The amounts of mutant/total mtDNA (expressed as a percentage) in various tissues in case 1 were as

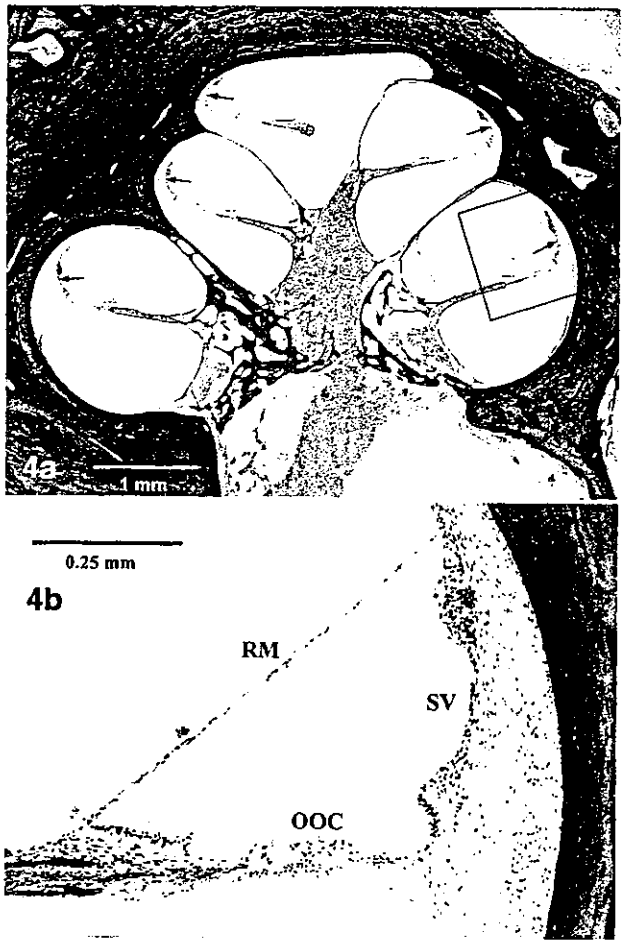

Fig. 4. Histopathological appearance of the right temporal bone of patient in case 2. (**A**) Mid-modiolar section of the cochlea showed diffuse, severe atrophy of the stria vascularis in all turns (arrows). There was no endolymphatic hydrops. (**B**) High-power view of the scala media from the basal turn showed severe atrophy of the stria vascularis (SV). The organ of Corti (OOC) including hair cells and supporting cells, the tectorial membrane, and Reissner's membrane (RM) appeared to be normal.

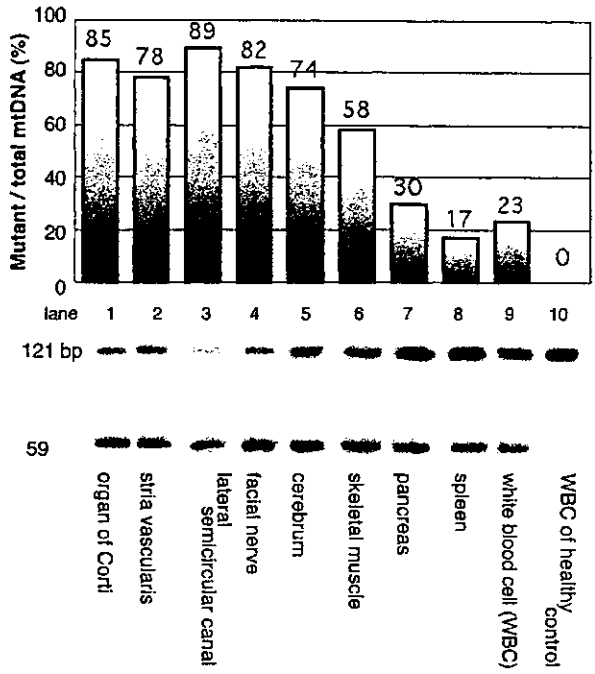

Fig. 5. Prevalence of mutant mitochondrial DNA (mtDNA) within various tissues, expressed as mutant/total mtDNA × 100%. (**Top**) Histogram of the mutant mtDNA. (**Bottom**) Gel electrophoresis. Normal and mutant mtDNA were detected as long (121 base pairs) and short (59 base pairs) bands, respectively. The inner ear tissues including the organ of Corti, stria vascularis, and lateral semicircular canal demonstrated high levels of mutant mtDNA ratio compared with other tissues.

follows: organ of Corti, 85%; stria vascularis, 78%; lateral semicircular canal, 89%; facial nerve, 82%; cerebrum, 74%; skeletal muscle, 58%; pancreas, 30%; spleen, 17%; and leukocytes, 23% (Fig. 5).

DISCUSSION

MELAS is associated with an A to G mutation at nucleotide 3243 in mtDNA in 80% to 90% of patients, and 30 to 70% of these patients have been reported to have SNHL.[4–6] The histopathology of the inner ear in MELAS has not been previously reported. However, there have been two reports describing the otopathological findings in related mitochondrial syndromes associated with SNHL. Lindsay and Hinojosa[15] described the otopathological findings in the temporal bones of a 19-year-old girl with Kearns-Sayre syndrome who had been deaf since age 6 years. The Kearns-Sayre syndrome is currently known to be the result of large deletions within mtDNA.[16] The case reported by Lindsay and Hinojosa with profound hearing loss showed bilateral, advanced cochleosaccular degeneration with complete absence of the organ of Corti, severe loss of the stria vascularis, collapse of Reissner's membrane, severe spiral ganglion cell loss, degeneration of the saccular macula, and normal cristae and utricle. Yamasoba et al.[17] reported the otopathological findings in a 56-year-old woman with maternally inherited diabetes and deafness (MIDD). There was severe loss of the stria vascularis, diffuse outer hair cell loss, spiral ganglion cell loss in the basal turn, and normal appearance of the saccule, utricle, and cristae. There was no collapse of Reissner's membrane. Yamasoba et al.[17] retrieved the DNA from archival temporal bone tissues and regarded the disorder as an A to G point mutation in mtDNA at the 3243 location.

The two cases with MELAS that we describe have certain features that make them valuable for study: a definitive molecular diagnosis was made during life, the SNHL was symmetrical and partial, and quantitative mitochondrial studies were performed in one of the two cases. Both cases showed a similar, diffuse and severe loss of the stria vascularis in all turns. There was a disproportional loss of spiral ganglion cells compared with loss of hair cells of the organ of Corti in case 1. In case 2, many spiral ganglion cells showed degenerative change, although the number of spiral ganglion cells was preserved. Although the organ of Corti showed some loss of hair cells in both cases, it was insufficient to explain the observed

loss of spiral ganglion cells as a secondary event. Thus, spiral ganglion cell loss appears to be a primary event in MELAS, rather than secondary degeneration resulting from hair cell loss. Within the normal cochlea the cells of the stria vascularis and the spiral ganglion contain large numbers of mitochondria per cell[18,19] and express high levels of Na-K-ATPase, an enzyme whose function requires energy produced by oxidative phosphorylation within mitochondria.[20,21] The 3243 mutation presumably disrupts mitochondrial oxidative phosphorylation, leading to reduced energy output and impaired cellular functioning. Our findings suggest that at least one major cause of SNHL in patients with MELAS is in the auditory periphery, involving dysfunction of the stria vascularis and spiral ganglion cells. This is consistent with clinical and audiological observations reporting benefit of both hearing aids and cochlear implantation in patients with MELAS.[22]

Though the cochlear pathological findings were similar in the two cases, the audiometric profiles were different, with a relatively flat SNHL in case 1 and downsloping SNHL in case 2. Dysfunction and atrophy of the stria vascularis are generally regarded to result in a relatively flat SNHL.[11] However, in theory, strial dysfunction can result in a downsloping SNHL as follows. Experimental induction of strial dysfunction by systemic administration of furosemide has been shown to cause a downsloping SNHL by decreasing the endocochlear potential (EP)[23] without a corresponding drop in endolymph potassium.[24] The decrease in EP causes threshold elevations and alterations in the tuning curves of auditory nerve fibers, and the basal fibers are affected far more than those in the more apical parts of the cochlea. Thus, it is conceivable that chronic strial dysfunction could result in a downsloping SNHL if it results in a decrease in EP without affecting the ability of the stria to maintain endolymphatic potassium.

Marked loss of neurons and severe gliosis in the ventral cochlear nuclei (VCN) were demonstrated in case 1. The degree and type of hearing loss caused by dysfunction of the VCN are not well established, although Armstrong et al.,[25] on the basis of one case, suggested that VCN loss may be responsible for high-tone SNHL. Our light microscopic studies showed that the remainders of the central auditory pathways were present in case 1, and all brainstem auditory structures were present in case 2. However, we must point out that quantitative studies were not conducted. It has been shown that central disease can manifest as reduction in cell volume and number of synapses without a reduction in number of neurons.[26] Hence, we cannot rule out central auditory dysfunction as an additional factor leading to SNHL in MELAS.

The vestibular otopathological findings in both cases were similar, and this contrasts with the cochlear otopathological findings. Both cases showed reduction in the numbers of hair cells in the cristae and maculae, with apparent preservation of the dark cells (although quantitative density counts of the dark cells were not conducted). The reduced caloric response during vestibular testing in case 1 can be accounted for by the reduction in hair cells within the lateral canal crista.

Our quantitative inner ear DNA studies showed that there was no correlation between the proportion of mutant to wild-type DNA and histological changes. For example, the percentages of mutant/total DNA were 78% in the stria and 89% in the lateral canal crista (both tissues were affected), whereas the percentages were 85% in the organ of Corti and 82% in the facial nerve (both tissues were unaffected). Another example of the lack of correlation between the percentage of mutant DNA and clinical dysfunction is also evident in the patient in case 1 who had severe diabetes with a low percentage (30%) of mutant/total DNA in the pancreas. The observed inconsistency between amounts of mutant DNA and tissue dysfunction has also been observed in other organs in MELAS, as well as in other mitochondrial disorders.[7–9,16] This inconsistency implies different thresholds of vulnerability to presumably similar impairments of oxidative phosphorylation, the so-called "threshold" effect.[7,8] Recent work has also demonstrated the phenomenon of "intermitochondrial complementation," which refers to the exchange of genetic information between mutant and normal mitochondria within a cell, so that the phenotypic expression of mutant mtDNA can be prevented by normal mtDNA.[27] It is obvious that more work is necessary to understand the differences in penetrance and tissue specificity in MELAS and in other mitochondrial disorders.

Histopathological and molecular studies of the inner ear pose special challenges, mainly because of the inaccessibility of the inner ear to direct examination or to biopsy during life. However, with the proper planning (as illustrated by the two cases in the present study), it is possible to perform both traditional light microscopic histopathological evaluations and more sophisticated quantitative DNA assessments on temporal bones acquired from patients with well-documented and defined genetic disorders. In addition, genomic DNA can be successfully extracted from archival, celloidin-embedded temporal bones and then sequenced to identify potential molecular defects in the inner ear.[28,29] An example of this latter approach for mtDNA deafness was the report of Yamasoba et al.[17] in identifying the 3243 mutation from an archival temporal bone with MIDD. The temporal bone collections in Europe and the United States contain approximately 8,000 and 13,000 specimens, respectively, representing a large archival repository of tissue that is available for molecular studies.[30,31]

CONCLUSION

The present study revealed severe degeneration of the stria vascularis and degenerative change of spiral ganglion cells in MELAS. The proportion of mutant to wild-type mtDNA was relatively high within the inner ear, which is similar in both histologically affected and histologically unaffected tissues. These findings suggest that dysfunction of the stria vascularis and spiral ganglion cells cause SNHL in MELAS.

Acknowledgments

The authors thank Joseph B. Nadol, Jr., MD, and Yoshihiko Murakami, MD, for their advice and comments; Kojiro Tuji, MD, Yasushi Kuroishikawa, MD, Hiro-oki

Okamura, MD, Mikio Sawada, MD, and Ritsuo Hashimoto, MD, for their technical assistance.

BIBLIOGRAPHY

1. Goto Y, Nonaka I, Horai S. A mutation in the tRNA(Leu)(UUR) gene associated with the MELAS subgroup of mitochondrial encephalomyopathies. *Nature* 1990;348: 651–653.
2. Kobayashi Y, Momoi MY, Tominaga K, et al. A point mutation in the mitochondrial tRNA(Leu)(UUR) gene in MELAS (mitochondrial myopathy, encephalopathy, lactic acidosis and stroke-like episodes). *Biochem Biophys Res Commun* 1990;173:816–822.
3. Pavlakis SG, Phillips PC, DiMauro S, DeVivo DC, Rowland LP. Mitochondrial myopathy, encephalopathy, lactic acidosis, and strokelike episodes: a distinctive clinical syndrome. *Ann Neurol* 1984;16:481–488.
4. Sue CM, Lipsett LJ, Crimmins DS, et al. Cochlear origin of hearing loss in MELAS syndrome. *Ann Neurol* 1998;43: 350–359.
5. Tamagawa Y, Kitamura K, Hagiwara H, et al. Audiologic findings in patients with a point mutation at nucleotide 3,243 of mitochondrial DNA. *Ann Otol Rhinol Laryngol* 1997;106:338–342.
6. Warrick PD, Wardrop P, Sim DW. Sensorineural hearing loss in MELAS syndrome. *J Laryngol Otol* 1997;111:279–281.
7. Ciafaloni E, Ricci E, Servidei S, et al. Widespread tissue distribution of a tRNALeu(UUR) mutation in the mitochondrial DNA of a patient with MELAS syndrome. *Neurology* 1991;41:1663–1664.
8. Hamazaki S, Koshiba M, Sugiyama T. Organ distribution of mutant mitochondrial tRNA(leu(UUR)) gene in a MELAS patient. *Acta Pathol Jpn* 1993;43:187–191.
9. Shiraiwa N, Ishii A, Iwamoto H, Mizusawa H, Kagawa Y, Ohta S. Content of mutant mitochondrial DNA and organ dysfunction in a patient with a MELAS subgroup of mitochondrial encephalomyopathies. *J Neurol Sci* 1993;120: 174–179.
10. Metz O. Threshold of reflex contractions of muscles of middle ear and recruitment of loudness. *Arch Otolaryngol* 1952; 55:536–543.
11. Schuknecht HF. Methods of removal, preparation, and study: correlation of function and pathology. In: *Pathology of the Ear*, ed 2, Pennsylvania: Lea and Febiger, 1993:21–29.
12. Velazquez-Villasenor L, Merchant SN, Tsuji K, Glynn RJ, Rauch SD. Temporal bone studies of the human peripheral vestibular system: normative Scarpa's ganglion cell data. *Ann Otol Rhinol Laryngol Suppl* 2000;181:14–19.
13. Yu GS, Otabe S, Niwa M. A sensitive fluorescent assay for the detection and quantification of mitochondrial 3243 mutation. *Rinsho Byori* 1996;44:778–782.
14. Scully RE, Mark EJ, McNeely WF, Ebeling SH. Weekly clinicopathological exercises, Case 39–1998: case records of the Massachusetts General Hospital. *N Engl J Med* 1998; 339:1914–1923.
15. Lindsay JR, Hinojosa R. Histopathologic features of the inner ear associated with Kearns-Sayre syndrome. *Arch Otolaryngol* 1976;102:747–752.
16. Wallace DC. Mitochondrial diseases in man and mouse. *Science* 1999;283:1482–1488.
17. Yamasoba T, Tsukuda K, Oka Y, Kobayashi T, Kaga K. Cochlear histopathology associated with mitochondrial transfer RNA(Leu(UUR)) gene mutation. *Neurology* 1999; 52:1705–1707.
18. Ross MD, Burkel W. Multipolar neurons in the spiral ganglion of the rat. *Acta Otolaryngol* 1973;76:381–394.
19. Sugar JO, Engstrom H, Stahle J. Stria vascularis. *Acta Otolaryngol Suppl* 1972;301:61–67.
20. Buffa P, Guarriera-Bobyleva V, Muscatello U, Pasquali-Ronchetti I. Conformational changes of mitochondria associated with uncoupling of oxidative phosphorylation in vivo and in vitro. *Nature* 1970;226:272–274.
21. Liberman EA, Topaly VP, Tsofina LM, Jasaitis AA, Skulachev VP. Mechanism of coupling of oxidative phosphorylation and the membrane potential of mitochondria. *Nature* 1969;222:1076–1078.
22. Rosenthal EL, Kileny PR, Boerst A, Telian SA. Successful cochlear implantation in a patient with MELAS syndrome. *Am J Otol* 1999;20:187–190.
23. Sewell WF. The effects of furosemide on the endocochlear potential and auditory-nerve fiber tuning curves in cats. *Hear Res* 1984;14:305–314.
24. Rybak LP, Morizono T. Effect of furosemide upon endolymph potassium concentration. *Hear Res* 1982;7:223–231.
25. Armstrong D, Stoney P, Hawke J, Farkashidy J. Presbycusis: correlations of clinical audiology with morphological changes in the cochlea and the ventral cochlear nucleus. *J Otolaryngol* 1992;21:343–349.
26. Powell TPS, Erulkar SD. Transneuronal cell degeneration in the auditory relay nuclei of the cat. *J Anat Lond* 1962;96: 249–268.
27. Nakada K, Inoue K, Ono T, et al. Inter-mitochondrial complementation: mitochondria-specific system preventing mice from expression of disease phenotypes by mutant mtDNA. *Nat Med* 2001;7:934–940.
28. McKenna MJ, Kristiansen A, Haines J. Isolation and identification of nucleic acid sequences from celloidin and paraffin embedded human temporal bone sections. In: *Immunobiology in Otorhinolaryngology: Progress of a Decade*. Amsterdam: Kugler, 1994:283–288.
29. Wackym PA, Simpson TA, Gantz BJ, Smith RJH. Polymerase chain reaction amplification of DNA from archival celloidin-embedded human temporal bone sections. *Laryngoscope* 1993;103:583–588.
30. Merchant SN, Schuknecht HF, Rauch SD, et al. The National Temporal Bone, Hearing, and Balance Pathology Resource Registry. *Arch Otolaryngol Head Neck Surg* 1993;119: 846–853.
31. Schuknecht HF. Temporal bone collections in Europe and the United States: observations on a productive laboratory, pathologic findings of clinical relevance, and recommendations. *Ann Otol Rhinol Laryngol Suppl* 1987;130:1–19.

Acta Neuropathol (2003) 106 : 112–120
DOI 10.1007/s00401-003-0708-z

REGULAR PAPER

Shinsuke Kato · Hiroshi Funakoshi · Toshikazu Nakamura · Masako Kato · Imaharu Nakano · Asao Hirano
Eisaku Ohama

Expression of hepatocyte growth factor and c-Met in the anterior horn cells of the spinal cord in the patients with amyotrophic lateral sclerosis (ALS): immunohistochemical studies on sporadic ALS and familial ALS with superoxide dismutase 1 gene mutation

Received: 15 October 2002 / Revised: 17 March 2003 / Accepted: 18 March 2003 / Published online: 18 April 2003
© Springer-Verlag 2003

Abstract To clarify the trophic mechanism of residual anterior horn cells affected by sporadic amyotrophic lateral sclerosis (SALS) and familial ALS (FALS) with superoxide dismutase 1 (SOD1) mutations, we investigated the immunohistochemical expression of hepatocyte growth factor (HGF), a novel neurotrophic factor, and its receptor, c-Met. In normal subjects, immunoreactivity to both anti-HGF and anti-c-Met antibodies was observed in almost all anterior horn cells, whereas no significant immunoreactivity was observed in astrocytes and oligodendrocytes. Histologically, the number of spinal anterior horn cells in ALS patients decreased along with disease progression. Immunohistochemically, the number of neurons negative for HGF and c-Met increased with ALS disease progression. However, throughout the course of the disease, certain residual anterior horn cells co-expressed both HGF and c-Met with the same, or even stronger intensity in comparison with those of normal subjects, irrespective of the reduction in the number of immunopositive cells. Western blot analysis revealed that c-Met was induced in the spinal cord of a patient with SALS after a clinical course of 2.5 years, whereas the level decreased in a SALS patient after a clinical course of 11 years 5 months. These results suggest that the autocrine and/or paracrine trophic support of the HGF-c-Met system contributes to the attenuation of the degeneration of residual anterior horn cells in ALS, while disruption of the neuronal HGF-c-Met system at an advanced disease stage accelerates cellular degeneration and/or the process of cell death. In SOD1-mutated FALS patients, Lewy body-like hyaline inclusions (LBHIs) in some residual anterior horn cells exhibited co-aggregation of both HGF and c-Met, although the cytoplasmic staining intensity for HGF and c-Met in the LBHI-bearing neurons was either weak or negative. Such sequestration of HGF and c-Met in LBHIs may suggest partial disruption of the HGF-c-Met system, thereby contributing to the acceleration of neuronal degeneration in FALS patients.

Keywords Amyotrophic lateral sclerosis · Hepatocyte growth factor · c-Met · Neurotrophic factor · Lewy body-like hyaline inclusion

S. Kato (✉) · E. Ohama
Department of Neuropathology, Institute of Neurological Sciences, Faculty of Medicine, Tottori University, Nishi-cho 36-1, 683-8504 Yonago, Japan
Tel.: +81-859-348034, Fax: +81-859-348289,
e-mail: kato@grape.med.tottori-u.ac.jp

H. Funakoshi · T. Nakamura
Division of Molecular Regenerative Medicine, Course of Advanced Medicine, Osaka University Graduate School of Medicine, 565-0871 Osaka, Japan

M. Kato
Division of Pathology, Tottori University Hospital, Yonago, Japan

I. Nakano
Department of Neurology, Jichi Medical College, Tochigi, Japan

A. Hirano
Division of Neuropathology, Department of Pathology, Montefiore Medical Center, Bronx, New York, USA

Introduction

Amyotrophic lateral sclerosis (ALS), which was first described by Charcot and Joffroy in 1869 [3], is a fatal and age-associated neurodegenerative disorder that primarily involves both the upper and lower motor neurons [11]. This disease has been recognized as a distinct clinicopathological entity of unknown etiology for over 130 years.

Hepatocyte growth factor (HGF) was first identified as a potent mitogen for mature hepatocytes [24] and was cloned in 1989 by Nakamura et al. [25]. Although HGF was discovered as a hepatotrophic factor, recent expression and functional analyses have revealed that HGF is also a neurotrophic factor [8, 21, 23]. HGF exerts neurotrophic effects on the hippocampal, cerebral cortical, midbrain dopaminergic, cerebellar granular, sensory, and motor neurons, as well as on the sympathetic neuroblasts [8, 12, 23]. HGF is one of the most potent *in vitro* survival-promoting

factors for motor neurons and is comparable to glial cell line-derived neurotrophic factor (GDNF) [6]. Neurotrophic effects have been demonstrated *in vivo* on embryonic spinal motor neurons during development and on adult motor neurons after axotomy of the hypoglossal nerve [27, 28, 40]. In addition, overexpression of neuronal HGF has been shown to result in the attenuation of neuronal cell death and progression of disease in a familial ALS (FALS) transgenic mouse model [35]. Therefore, HGF and its receptor, c-Met [9], might be beneficial for motor neuron survival.

An essential histopathological feature of ALS is loss of the large anterior horn cells throughout the spinal cord, and the surviving motor neurons of the spinal cord often exhibit shrinkage. Among these residual large anterior horn cells, some appear to be normal. These surviving neurons in ALS patients are thought to possess some form of self-preservation mechanism. To gain new insight into the survival/trophic mechanism of these residual neurons, we focused on the HGF-c-Met system. To date, there have been no reports demonstrating the immunohistochemical expression of HGF and c-Met in motor neurons of the human ALS spinal cord. In the study presented here, we performed immunohistochemical analyses of the human spinal cord, not only from FALS patients with superoxide dismutase 1 (SOD1) gene mutations, but also from patients with sporadic ALS (SALS), and analyzed the expression of HGF and c-Met.

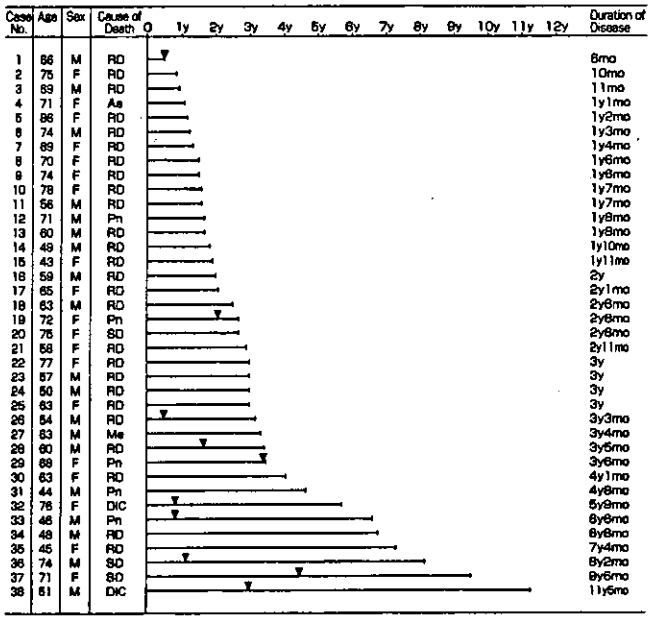

Fig. 1 Characteristics of 38 sporadic ALS cases. This figure includes each patient's age, sex, cause of death, and disease duration. The horizontal lines each show the duration of disease. Arrowheads indicate the time point at which the patients were placed on respirators. (*ALS* amyotrophic lateral sclerosis, *RD* respiratory distress, *As* asphyxia, *Pn* pneumonia, *SD* sudden death, *Me* melena, *DIC* disseminated intravascular coagulation, *y* years, *mo* months)

Materials and methods

Autopsy specimens

Immunohistochemical studies were performed on archival, buffered 10% formalin-fixed, paraffin-embedded spinal cord tissues obtained at autopsy from 38 SALS patients and 5 FALS patients who were members of two different families. The main clinical characteristics of the SALS patients are summarized in Fig. 1. The clinicopathological characteristics of the FALS patients are summarized in Table 1 and have been reported previously [14, 15, 18, 19, 26, 33, 36]. SOD1 analysis revealed that the members of the Japanese Oki family had a two-base pair deletion at codon 126 (frameshift 126 mutation) [14] and that the members of the American C family had an Ala to Val substitution at codon 4 (A4V) [33]. We also examined autopsy specimens of the spinal cord from 20 neurologically and neuropathologically normal individuals (11 males, 9 females; aged 37–75 years). This study was approved by the Ethics Committee of Tottori University (Permission No. 2001-150).

Histopathology and immunohistochemistry

After fixation in buffered 10% formalin, the specimens were paraffin-embedded, cut into 6-μm-thick sections, and examined by light microscopy. Spinal cord sections were subjected to routine staining with hematoxylin and eosin (H-E), Klüver-Barrera, Holzer, and Bielschowsky stains. Representative paraffin sections were used for immunohistochemical staining with the following primary antibodies: an affinity-purified rabbit antibody against human recombinant HGF purified from the culture medium of a Chinese hamster ovary cell that had been transfected with the human HGF expression vector (concentration: 5 μg/ml), and an affinity-purified rabbit antibody to human c-Met (C-12) [diluted 1:500 in 1% bovine serum albumin-containing phosphate-buffered saline (BSA-PBS), pH 7.4] (Santa Cruz Biotechnology, Santa Cruz, CA). Sections were deparaffinized, and endogenous peroxidase activity was quenched by incubation for 30 min with 0.3% H_2O_2. The sections were then washed in PBS. Normal serum homologous with the secondary antibody was used as a blocking reagent. Tissue sections were incubated with the primary antibodies for 18 h at 4°C.

Table 1 Characteristics of five FALS cases (*FALS* familial amyotrophic lateral sclerosis, *SOD* superoxide dismutase, *LBHI* Lewy body-like hyaline inclusion, *mo* months, *y* years, *2-bp* two-base pair, *PCI* posterior column involvement type, + detected, *ND* not determined, *As* asphyxia, *IH* intraperitoneal hemorrhage, *RD* respiratory distress, *Pn* pneumonia)

Case	Age	Sex	Cause of death	FALS duration	SOD1 mutation	Subtype	Neuronal LBHI
Japanese Oki family							
1	46	F	As	18 mo	2-bp deletion (126)	PCI	+
2	65	M	IH	11 y	2-bp deletion (126)	PCI and degeneration of other systems	+
American C family							
3	39	M	RD	7 mo	A4V	PCI	+
4	46	M	Pn	8 mo	A4V	PCI	+
5	66	M	Pn	1 y	ND	PCI	+

PBS-exposed sections served as controls. For the preabsorption test, some sections were incubated with the anti-HGF antibody that had been preabsorbed with an excess amount of human recombinant HGF. Bound antibodies were visualized by the avidin-biotin-immunoperoxidase complex (ABC) method using the appropriate Vectastain ABC Kit (Vector Laboratories, Burlingame, CA) and 3,3'-diaminobenzidine tetrahydrochloride (DAB; Dako, Glostrup, Denmark) as the chromogen.

Western blot analysis

This analysis was carried out on three fresh autopsy specimens from spinal cord cervical segments: two SALS cases [2.5 years after onset (case 18 in Fig. 1, age 63 years) and 11 years 5 months after onset (case 38 in Fig. 1, age 51 years)], and one normal individual (age 68 years). In brief, specimens were homogenized in Laemmli sample buffer (Bio-Rad, Hercules, CA) containing 2% sodium dodecyl sulfate (SDS), 25% glycerol, 10% 2-mercaptoethanol, 0.01% bromophenol blue, and 62.5 mM TRIS-HCl (pH 6.8). The samples were heated at 100°C for 5 min. Soluble protein extracts (20 μg) from the samples were separated on SDS-polyacrylamide gels (4%–20% gradient, Bio-Rad) and transferred by electroblotting to Immobilon PVDF (Millipore, Bedford, MA). After blocking with 5% nonfat milk for 30 min at room temperature, the blots were incubated overnight at 4°C with the antibodies against human HGF and c-Met. Binding to HGF and c-Met was visualized with the Vectastain ABC Kit and DAB. Appropriate molecular weight markers (Bio-Rad) were included in each run.

Results

Histopathology

An essential histopathological finding of the spinal cord in ALS was loss of motor neurons throughout the course of the disease. In the specimens we examined, neuronal loss was most easily recognized in the cervical and lumbar enlargements. The surviving motor neurons showed shrinkage, and lipofuscin granule-filled neurons stood out. Among these residual motor neurons, some that were smaller in size appeared normal. The number of motor neurons decreased with ALS disease progression. Reactive astrocytosis and gliosis were also observed in the affected areas. In the affected antero-lateral columns that were most pronounced in the crossed and uncrossed corticospinal tracts, there was a loss of large myelinated fibers in association

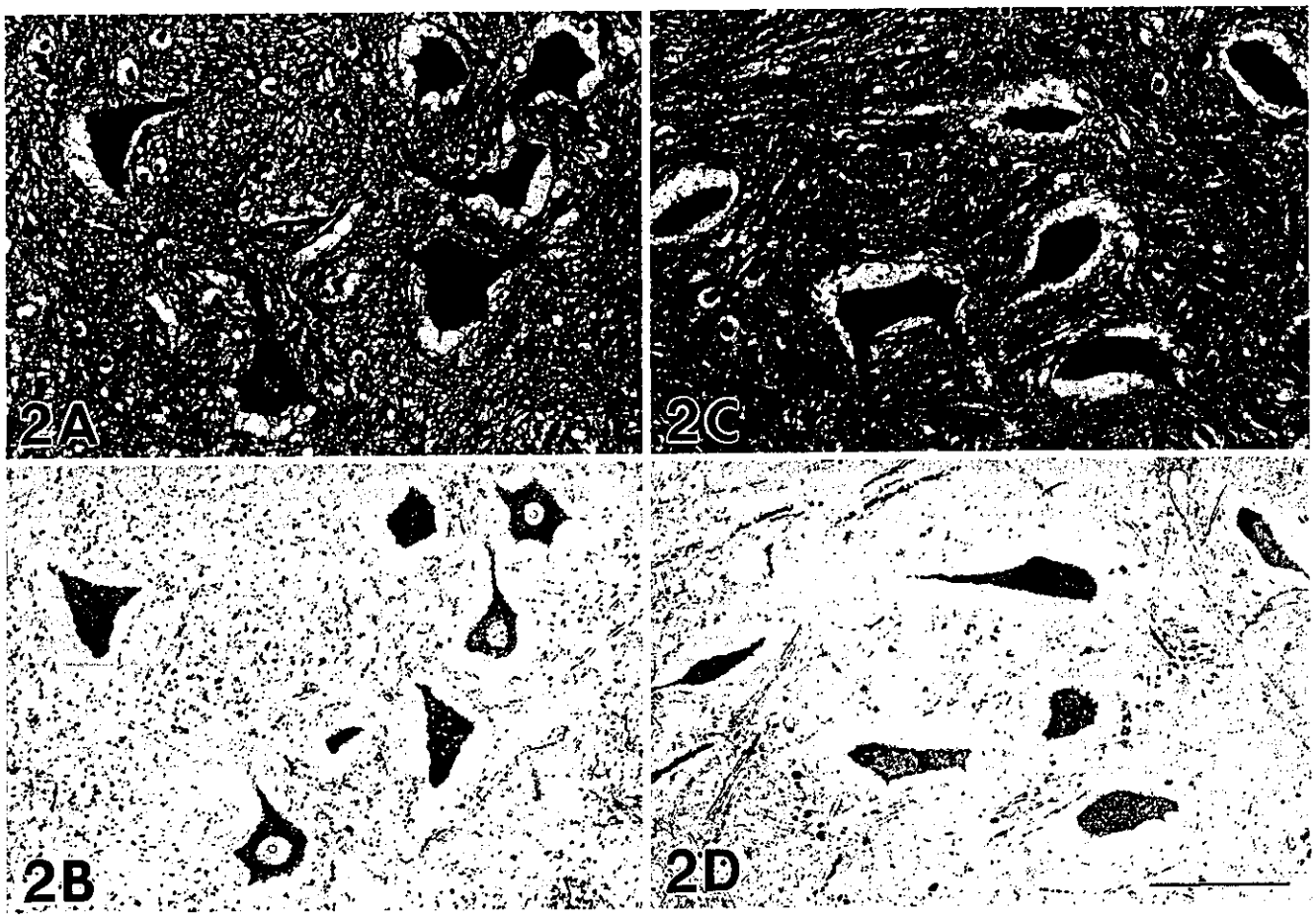

Fig. 2 Detection of HGF and its receptor, c-Met, in the normal anterior horn cells of the spinal cord. **A** Light microscopic preparation of the anterior horn cells stained with H-E. **B** Immunostaining with an antibody against HGF of the section consecutive to that shown in **A**. HGF immunoreactivity is identified in almost all of the motor neurons. Cytoplasmic staining is observed. No counterstaining. **C** Normal anterior horn cells stained with H-E. **D** Immunoreactivity for c-Met of the serial section of that shown in **C**. Almost all of the normal motor neurons are immunopositive for c-Met. Diffuse staining of the cell bodies and proximal dendrites is evident. No counterstaining. (*HGF* hepatocyte growth factor, *H-E* hematoxylin and eosin). *Bar* **A–D** 100 μm

with variable degrees of astrocytic gliosis. Fiber destruction was associated with the appearance of lipid-laden macrophages.

Analysis of the essential changes in the five cases of FALS revealed a subtype of FALS with posterior column involvement (PCI). This subtype is characterized by degeneration of the middle root zones of the posterior column, Clarke nuclei, and the posterior spinocerebellar tracts, in addition to spinal cord motor neuron lesions. A patient who had survived for a long period, with a clinical course of 11 years (case 2 in Table 1), showed multi-system degeneration in addition to the features of FALS with PCI. Neuronal Lewy body-like hyaline inclusions (LBHIs) were present in all five FALS cases.

The spinal cords of normal individuals did not exhibit any distinct histopathological alterations.

Immunohistochemistry

When control and representative paraffin sections were incubated with PBS alone (i.e., no primary antibody), no staining was detected. In addition, incubation of sections with anti-HGF antibody that had been pretreated with an excess of recombinant human HGF produced no staining in any of the sections. HGF immunoreactivity in normal spinal cords was identified in almost all of the motor neurons: cytoplasmic staining was observed with various staining intensities (Fig. 2A, B). A similar staining pattern was also observed for c-Met, the cell bodies and proximal dendrites being stained (Fig. 2C, D). Almost all of the motor neurons in normal spinal cords co-expressed both HGF and c-Met, although the staining intensity of positively stained neurons varied. No significant immunoreactivity for HGF and c-Met was seen in astrocytes and oligodendrocytes from normal subjects.

As for the anterior horn cells in ALS patients, some residual neurons expressed both HGF and c-Met strongly within about 2 years of disease onset (cases 1–15 in Fig. 1). Both antibodies produced a cytoplasmic staining pattern. Other neurons were either faintly stained by both antibodies or unstained. Around 2–3 years after disease onset in ALS patients (cases 16–25 in Fig. 1), the intensity of HGF and c-Met immunoreactivity peaked in some neurons that were positive for both proteins (Fig. 3). In ALS patients with a clinical course of over 3 years (cases 26–38 in Fig. 1), the number of residual neurons decreased strikingly, and respiratory assistance became essential for most patients; the residual neurons intensely expressing both HGF and c-Met decreased with disease progression, while the number of residual neurons negative for both proteins increased dramatically (Fig. 4). At 11 years 5 months after disease onset (case 38 in Fig. 1), although a small number of residual neurons were still evident, most of them were atrophic and immunonegative for both HGF and c-Met. However, even in this long-surviving patient, a few residual neurons expressing both HGF and c-Met were observed (Fig. 5). Thus, residual neurons that were positive for both HGF and c-Met were present throughout the disease course in every ALS patient. Expression of HGF and c-Met by only part of the neuronal cytoplasm and/or dendrites was observed more often as ALS-associated degeneration progressed (Figs. 4, 5). Observation of only the H-E-stained sections revealed no difference between the neurons positive for HGF and c-Met and those negative for both proteins (Figs. 4, 5).

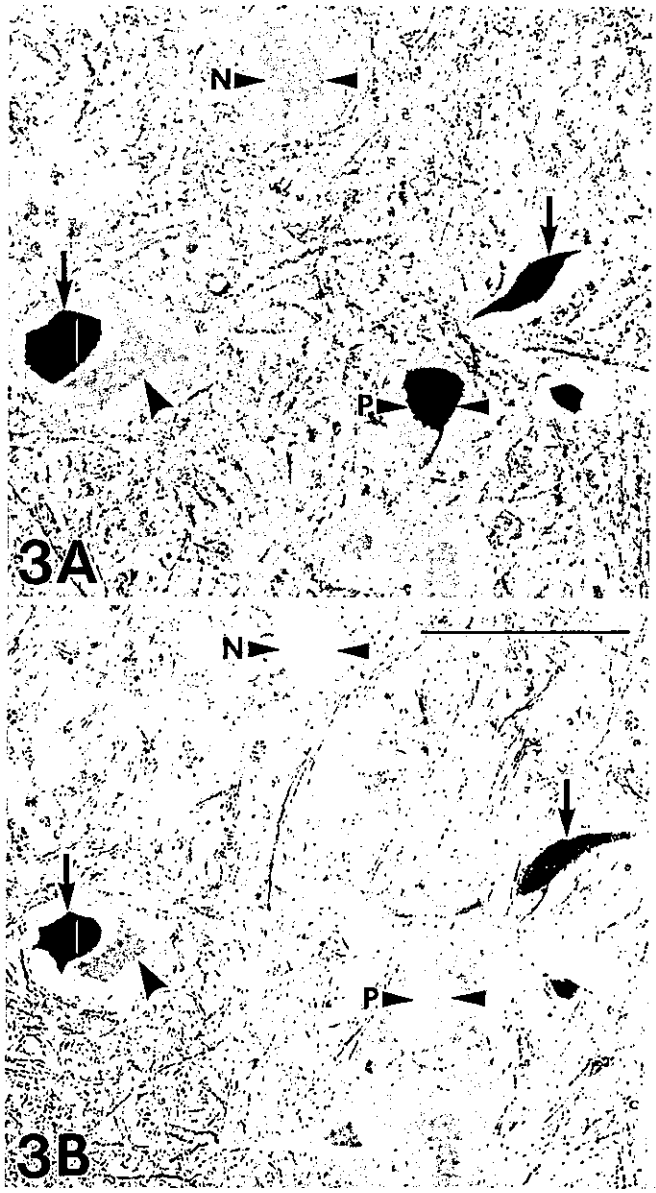

Fig. 3 Serial sections of spinal anterior horn cells in a patient with sporadic ALS after a clinical course of 2.5 years (case 18 in Fig. 1) immunostained with antibodies against HGF (**A**) and c-Met (**B**). Residual neurons intensely expressing both HGF and c-Met are evident (*arrows*). The staining pattern is diffuse in the cytoplasm. Other neurons are either faintly stained by both antibodies, or unstained (*big arrowhead*). However, neither the HGF-positive neuron (*small arrowheads* with *P*) nor the HGF-negative neuron (*small arrowheads* with *N*) in the HGF section shown in **A** appears in the section stained for c-Met in **B**. No counterstaining. *Bar* **B** (also for **A**) 100 μm

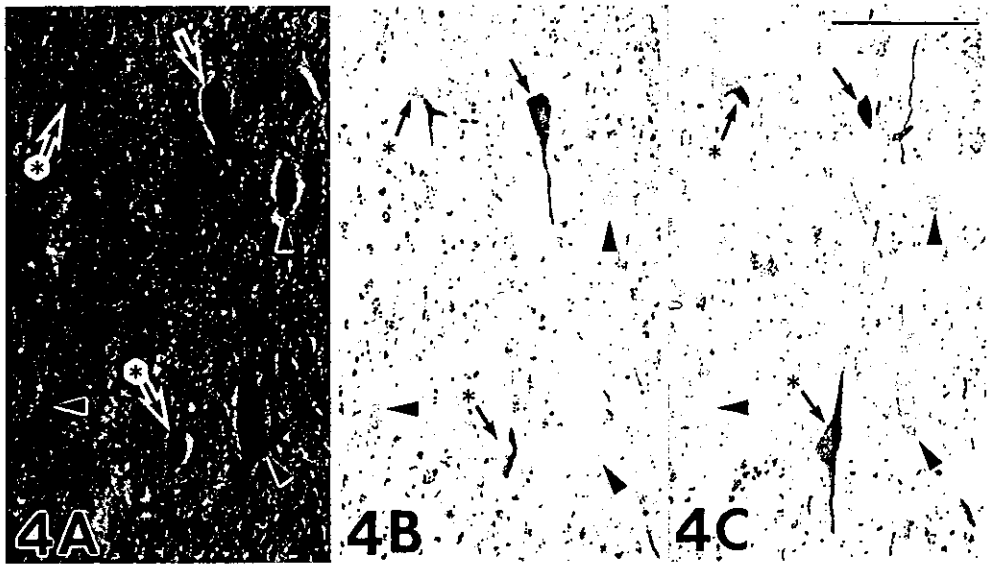

Fig. 4 Serial sections of the anterior horn cells in a patient with sporadic ALS after a clinical course of 4 years 8 months (case 31 in Fig. 1). **A** In the H-E preparation, residual motor neurons appear to be atrophic. There is no distinction among these atrophic neurons when observed in the H-E preparation alone. **B** Immunostaining with the antibody against HGF. The number of residual neurons intensely expressing HGF (*arrow*) is reduced in comparison with that in the ALS patient after a clinical course of 2.5 years (Fig. 3). Only part of the neuronal cell body and dendrite expresses HGF (*arrows* and *asterisks*). The number of HGF-negative neurons is increased (*arrowheads*). No counterstaining. **C** Immunostaining with the c-Met antibody. Similarly to the anti-HGF immunostaining, the number of c-Met-immunopositive neurons is diminished (*arrow*). In contrast, the number of c-Met-immunonegative neurons is increased (*arrowheads*). However, only part of the neuronal cytoplasm and dendrite is positive for c-Met (*arrows* and *asterisks*). No counterstaining. *Bar* **C** (also for **A**, **B**) 100 μm

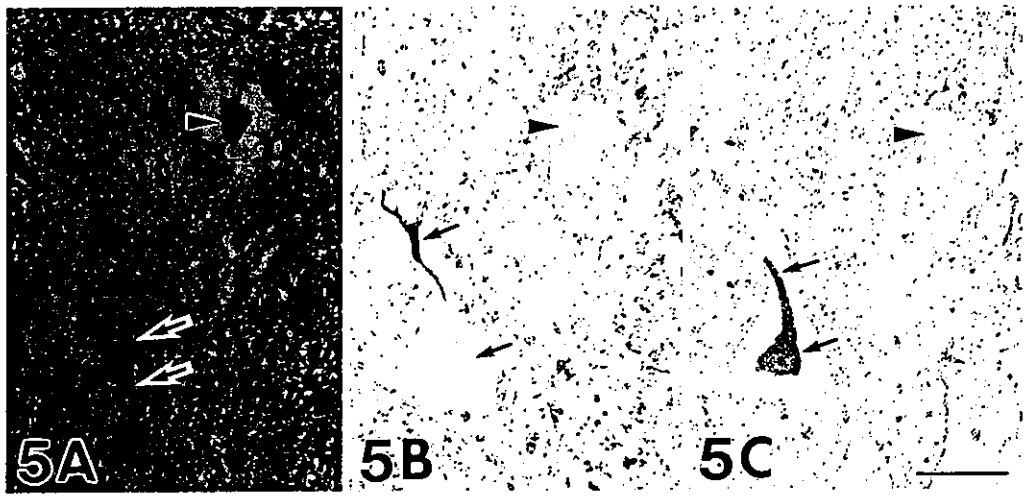

Fig. 5 Expression of HGF and c-Met detected by immunohistochemistry in a patient with sporadic ALS after a clinical course of 11 years 5 months (case 38 in Fig. 1). **A** Light microscopic preparation stained with H-E. Small and atrophic motor neurons are seen. **B** HGF immunoreactivity of the section consecutive to that shown in **A**. Although the residual neuron (*double arrows*) appears to be atrophic in the H-E preparation, this residual neuron expresses HGF: only a dendrite is HGF-positive (*double arrows*). No counterstaining. **C** c-Met immunoreactivity of the section consecutive to that shown in **B**. The residual neuron that appears to be atrophic in the H-E preparation is stained by the anti-c-Met antibody (*double arrows*). A neuron negative for both HGF and c-Met can be also observed (*arrowhead*). No counterstaining. Observation of the H-E-stained section in **A** reveals no difference between the atrophic neuron positive for HGF and c-Met (indicated by *double arrows*) and the atrophic neuron negative for both proteins (marked by an *arrowhead*). *Bar* **C** (also for **A**, **B**) 50 μm

With respect to the LBHI-bearing neurons in the anterior horns of FALS patients with SOD1 mutations, LBHIs in the anterior horn cells showed co-aggregation of both HGF and c-Met (Fig. 6). However, the intensity of cytoplasmic HGF and c-Met staining in LBHI-bearing neurons was either weak or negative. Except for the LBHI-bearing neurons, the stainability and intensity of HGF and c-Met staining in the residual neurons of SOD1-mutated FALS patients were identical to those of the SALS patients.

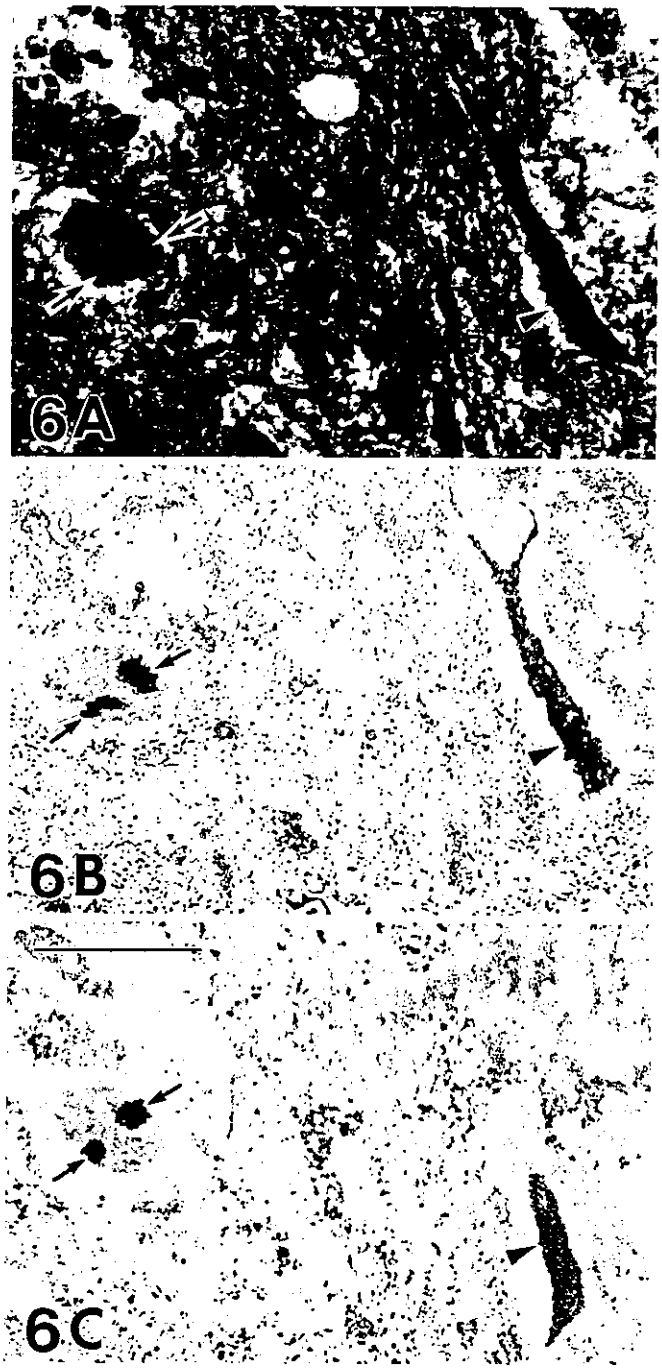

Fig. 6 Serial sections of neuronal LBHIs in a familial ALS patient with an SOD1 mutation (case 2 in Table 1). **A** In the H-E preparation, the neuronal LBHIs consist of eosinophilic cores with paler peripheral halos (*arrows*). An atrophic anterior horn cell without inclusions is also seen (*arrowhead*). **B** Immunostaining with the c-Met antibody is strongly positive for the neuronal LBHI core (*arrows*). However, the cytoplasmic staining intensity of the LBHI-bearing neuron is weak. By contrast, c-Met expression is evident even in the atrophic neuron (*arrowhead*). No counterstaining. **C** Immunostaining with the HGF antibody. The LBHIs show co-aggregation of both HGF and c-Met (*arrows*). Even though the cytoplasm of the shrunken neuron is positive for both HGF and c-Met (*arrowhead*), the cytoplasmic staining intensity of the LBHI-bearing neuron to HGF and c-Met is weak. No counterstaining. (*LBHI* Lewy body-like hyaline inclusion, *SOD1* superoxide dismutase 1). *Bar* **C** (also for **A**, **B**) 50 μm

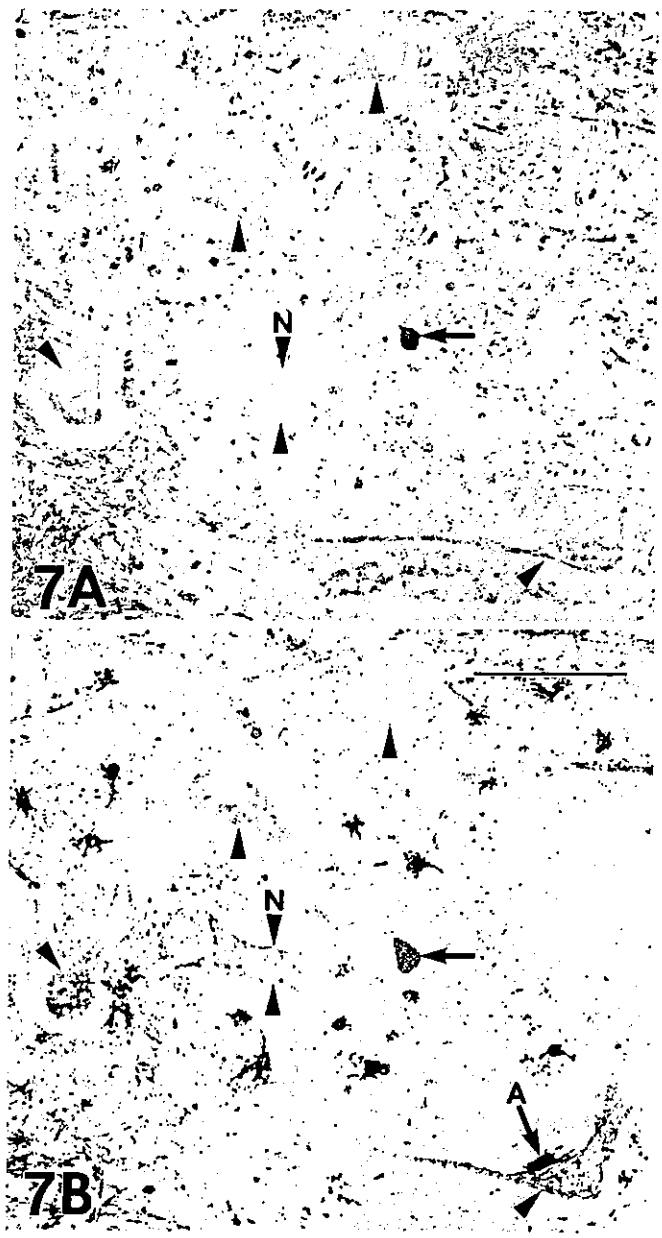

Fig. 7 HGF and c-Met expression in reactive astrocytes in a patient with sporadic ALS after a clinical course of 4 years 1 month (case 30 in Fig. 1). **A** Although only part of the neuronal cytoplasm is HGF-positive (*arrow*), almost all of the neurons are either faintly stained by the anti-HGF antibody, or not at all (*arrowheads*). No significant HGF immunoreactivity is evident in astrocytes. No counterstaining. **B** c-Met immunoreactivity of the section consecutive to that shown in **A**. c-Met expression is observed in reactive astrocytes. In general, c-Met-positive reactive astrocytes are frequently present around the neurons negative for HGF and c-Met (*arrowheads*). An astrocyte in contact with a neuron negative for both proteins intensely expresses c-Met (*arrow* and *A*). Only part of the neuronal cytoplasm is immunopositive for HGF and c-Met (*arrow*). A c-Met-negative neuron (*arrowheads* and *N*) in the section stained for c-Met in **B** does not appear in the section stained for HGF in **A**. No counterstaining. *Bar* **B** (also for **A**) 100 μm

Although no significant HGF immunoreactivity was found in reactive astrocytes in any of the ALS patients throughout the disease course, c-Met was expressed in these cells. These c-Met-positive reactive astrocytes were frequently seen around neurons that were negative for HGF and c-Met (Fig. 7). Reactive astrocytes in contact with neurons negative for both proteins showed intense expression of c-Met. The number of reactive astrocytes expressing c-Met tended to reach a peak around 3–4 years after ALS onset (Fig. 7), and thereafter decreased along with disease progression after patients had begun to require respiratory assistance. Oligodendrocytes showed no significant expression of HGF and c-Met.

Western blot analysis

When the tissue homogenate of each fresh cervical segment of the spinal cord was examined by immunoblotting for HGF, double bands at positions corresponding to approximately 34 kDa and 69 kDa were observed, i.e., those with the same mobility as human HGF (Fig. 8A). Immunoblotting showed that the intensity of HGF immunoreactivity in the SALS patient with a clinical course of 2.5 years (case 18 in Fig. 1) appeared to be identical to, or slightly stronger than, that in a normal subject. In the SALS patient with a clinical course of 11 years 5 months (case 38 in Fig. 1), HGF expression was less than that in the normal subject. This observation supported the results of HGF immunohistochemistry.

Immunoblotting for c-Met revealed a single band corresponding to about 140 kDa in two SALS cases and a normal subject (Fig. 8B). This molecular mass was compatible with that of human c-Met. In the SALS case at 2.5 years after disease onset (case 18 in Fig. 1), c-Met was expressed more strongly than in the normal subject. However, the level of c-Met expression in the SALS case at 11 years 5 months after onset (case 38 in Fig. 1) decreased below that in the normal subject. This finding reflected the c-Met immunohistochemistry results.

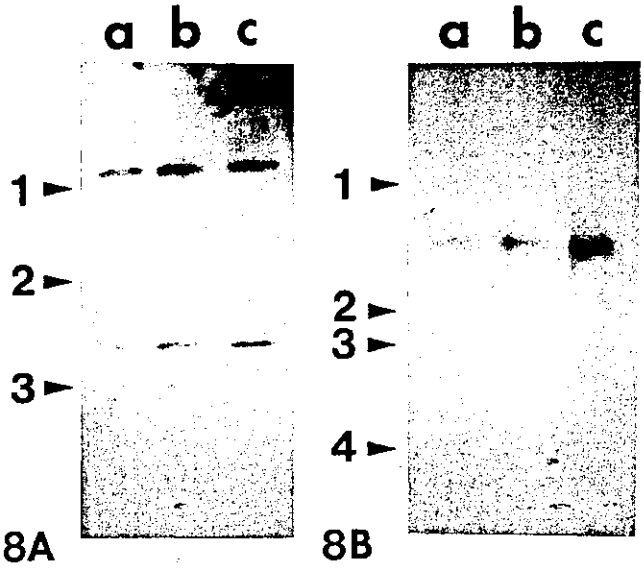

Fig. 8 Western blot analyses using the antibodies against HGF (**A**) and c-Met (**B**). A 20-μg amount of the soluble protein extract from each sample has been applied to each lane. A Molecular mass markers: *1* bovine serum albumin (66 kDa); *2* ovalbumin (45 kDa); *3* carbonic anhydrase (31 kDa). *Lane a* A sporadic ALS patient with a clinical course of 11 years 5 months (case 38 in Fig. 1), *lane b*: normal control, *lane c*: a sporadic ALS patient with a clinical course of 2.5 years (case 18 in Fig. 1). Double bands with molecular masses of approximately 69 kDa and 34 kDa are observed in all samples. The intensity of HGF immunoreactivity in *lane c* (ALS case 18) appears to be identical to, or slightly stronger than, that in *lane b* (normal). In contrast, HGF expression in *lane a* (ALS case 38) appears to be lower than that in *lane b* (normal). **B** Molecular mass markers: *1* myosin (200 kDa); *2* β-galactosidase (116 kDa); *3* phosphorylase B (97.4 kDa); *4* bovine serum albumin (66 kDa). A single band corresponding to about 140 kDa is detected in each sample. Expression of c-Met in *lane c* (case 18) is stronger than in *lane b* (normal). However, the level of c-Met expression in *lane a* (case 38) is decreased below that seen in *lane b* (normal)

Discussion

HGF is a heterodimeric protein composed of two polypeptide chains (69 kDa α chain and 34 kDa β chain) linked together by disulfide bonds [25]. HGF has four intrachain disulfide loops, called "kringle" domains, in its α chain [25]. In vitro, HGF is one of the most potent neurotrophic factors for motor neurons [6]. The HGF antibody used in the present study recognizes both the α and β chains. HGF acts via its receptor, c-Met, which is a transmembrane protein of 190 kDa, consisting of a 50-kDa extracellular α subunit and a 140-kDa β subunit with a tyrosine kinase domain [29]. According to the manufacturer (Santa Cruz), the c-Met antibody recognizes only the β subunit. This is consistent with the results of Western blot analyses, where use of a normal tissue homogenate yielded double bands of approximately 69 kDa and 34 kDa with the anti-HGF antibody, and a single band of about 140 kDa with the anti-c-Met antibody.

Under normal physiological conditions, HGF and c-Met immunoreactivity in the human spinal cord anterior horns was primarily identified in the neurons: cytoplasmic staining with antibodies against both proteins was observed in almost all of the anterior horn cells. Considering that HGF has extremely potent neurotrophic activity and acts through c-Met, our immunohistochemical findings indicate that even under normal physiological conditions, spinal motor neurons maintain themselves via an HGF-c-Met autocrine and/or paracrine system. No significant HGF and c-Met immunoreactions were seen in astrocytes and oligodendrocytes. Even if the astrocytes and oligodendrocytes produced only infinitesimal traces of HGF and c-Met, the protein production levels were below the limits of immunohistochemical detection.

A very striking feature was the presence of certain residual motoneurons intensely co-expressing both HGF and c-Met throughout the disease course of ALS. This suggests that the HGF-c-Met system may represent an endogenous survival mechanism that is activated by ALS

stress. Although some neurons co-expressed HGF-c-Met, while many were negative for both proteins among the residual motoneurons affected by ALS, there was no apparent difference among these residual ALS neurons when observed in H-E preparations alone. Those residual neurons showing high co-expression of HGF and c-Met would be less susceptible to ALS stress and protect themselves from ALS neuronal death. In addition, the residual neurons that are immunopositive for HGF and c-Met might maintain their viability via an autocrine and/or paracrine mechanism involving the HGF-c-Met system. This hypothesis is supported by the fact that HGF is one of the most potent survival-promoting factors for motor neurons, being comparable to GDNF in vitro [6]. Because of the neurite outgrowth-promoting property of HGF in vitro [7, 10, 22], residual neurons that are immunoreactive for HGF and c-Met might show enhanced neurite outgrowth to other neurons and regenerate the neuronal network to compensate for any functional deficiency and neuron loss. In other words, those motor neurons showing up-regulation of the HGF-c-Met cell-survival system, which is normally present in neurons, might show enhanced cell survival in the presence of ALS stress. In contrast, breakdown of the HGF-c-Met system in ALS motor neurons that are barely viable would result in cell death, and many residual neurons that are unable to express HGF and c-Met would be ultimately moribund. It remains to be determined whether this HGF-c-Met up-regulation is a direct or an indirect effect based on the pathogenesis of ALS itself, or whether HGF and c-Met play a primary or a secondary role in attenuating ALS-related neuronal death.

Focusing on FALS with SOD1 mutations, the SOD1 protein (probably the mutant form) aggregates in the anterior horn cells as neuronal LBHIs [14, 15, 33]. It is of great interest that these LBHIs corresponded to structures immunostained by both antibodies against HGF and c-Met. The cytoplasm of these LBHI-bearing neurons was only weakly immunopositive, or even immunonegative, for HGF and c-Met. Such sequestration into LBHIs has also been observed for normal constitutive proteins such as tubulin and tau protein [15, 16, 17], and this resulted in partial impairment of the maintenance of cell metabolism [15, 16, 17]. Although we cannot readily compare the sequestration of normal constitutive proteins with internalization of a cell-survival ligand-receptor system like HGF and c-Met, these findings lead us to speculate that internalization of HGF and c-Met into LBHIs in FALS patients may partly contribute to the breakdown of HGF autocrine and/or paracrine trophic support in these neurons and may be one of the endogenous mechanisms that accelerate neuronal death. This hypothesis would appear to be compatible with the aggregation toxicity theory.

Reactive astrocytosis and gliosis were observed in the anterior horns of patients with SALS and FALS. Based on observations of H-E preparations alone, these findings suggest that the reactive astrocytes merely fill the spaces created by neuronal loss. It is noteworthy that these reactive astrocytes in both types of ALS expressed c-Met. Thus, it appears that c-Met induction in reactive astrocytes is a common feature in ALS patients. It should be noted that astrocytes, in contact to neurons that were immunonegative for both proteins, intensely expressed c-Met. This may reflect c-Met regulation in astrocytes through an astrocyte-neuron relationship. Astrocytes play important roles in sustaining environments within the central nervous system, including neuronal maintenance [20, 32, 34, 37, 39]. Neuronal vulnerability to oxidative stress or toxicity is greater in neurons cultured alone than in neurons co-cultured with astrocytes [4, 5]. It has been shown that the activity of the glial-specific glutamate transporter (EAAT2/GLT1) in spinal cord astrocytes is selectively diminished in human SALS [30, 31] as well as in the SOD1-mutated ALS model transgenic animals of G85R [2], A4V [38], I113T [38], and G93A [1, 13]. Therefore, it can be postulated that HGF might protect c-Met-positive reactive astrocytes from down-regulation of the glial-specific glutamate transporter (EAAT2) via the HGF-c-Met system, and increase glutamate clearance, thereby leading to a reduction in glutamatergic neurotoxicity and resulting in promotion of neuronal survival [35]. However, 3–4 years after ALS onset, the number of c-Met-positiv reactive astrocytes decreased along with disease progression. These findings suggest that breakdown of the HGF-c-Met system is involved in the impairment of both astrocytic function itself and astrocyte-neuron relationship at the terminal stage of ALS. It remains to be determined whether this consideration applies to a degenerative condition such as ALS, in which affected astrocytes do not have a normal control mechanism. Taken together with the fact that overexpression of HGF has been reported to attenuate motor neuron death and prolong the life-span of FALS transgenic mouse model [35], our data in this report may lead to the development of a new HGF-based therapy for ALS, which for over 130 years has had an unknown etiology.

Acknowledgements This study was supported in part by a Grant-in-Aid for Scientific Research (c) (2) from the Ministry of Education, Culture, Sports, Science and Technology for Japan (S.K.: 13680821) and by a Grant from the Ministry of Health, Labor and Welfare (S.K. and H.F.).

References

1. Bendotti C, Tortarolo M, Suchak SK, Calvaresi N, Carvelli L, Bastone A, Rizzi M, Rattray M, Mennini T (2001) Transgenic SOD1 G93A mice develop reduced GLT-1 in spinal cord without alterations in cerebrospinal fluid glutamate levels. J Neurochem 79:737–746
2. Bruijn LI, Becher MW, Lee MK, Anderson KL, Jenkins NA, Copeland NG, Sisodia SS, Rothstein JD, Borchelt DR, Price DL, Cleveland DW (1997) ALS-linked SOD1 mutant G85R mediates damage to astrocytes and promotes rapidly progressive disease with SOD1-containing inclusions. Neuron 18:327–338
3. Charcot JM, Joffroy A (1869) Deux cas d'atrophie musculaire progressive avec lésions de la substance grise et des faisceaux antéro-latéraux de la moelle épinière. Arch Physiol (Paris) 2: 744–760
4. Dawson VL, Brahmbhatt HP, Mong JA, Dawson TM (1994) Expression of inducible nitric oxide synthase causes delayed neurotoxicity in primary mixed neuronal-glial cortical cultures. Neuropharmacology 33:1425–1430

5. Desagher S, Glowinski J, Premont J (1996) Astrocytes protect neurons from hydrogen peroxide toxicity. J Neurosci 16:2553–2562
6. Ebens A, Brose K, Leonardo ED, Hanson MG Jr, Bladt F, Birchmeier C, Barres BA, Tessier-Lavigne M (1996) Hepatocyte growth factor/scatter factor is an axonal chemoattractant and a neurotrophic factor for spinal motor neurons. Neuron 17: 1157–1172
7. Funakoshi H, Nakamura T (2001) Identification of HGF-like protein as a novel neurotrophic factor for avian dorsal root ganglion sensory neurons. Biochem Biophys Res Commun 283: 606–612
8. Funakoshi H, Nakamura T (2003) Hepatocyte growth factor (HGF): from diagnosis to clinical applications. Clin Chim Acta 327:1–23
9. Giordano S, Di Renzo MF, Narsimhan RP, Cooper CS, Rosa C, Comoglio PM (1989) Biosynthesis of the protein encoded by the c-met proto-oncogene. Oncogene 4:1383–1388
10. Hamanoue M, Takemoto N, Matsumoto K, Nakamura T, Nakajima K, Kohsaka S (1996) Neurotrophic effect of hepatocyte growth factor on central nervous system neurons in vitro. J Neurosci Res 43:554–564
11. Hirano A (1996) Neuropathology of ALS: an overview. Neurology 47:S63–S66
12. Honda S, Kagoshima M, Wanaka A, Tohyama M, Matsumoto K, Nakamura T (1995) Localization and functional coupling of HGF and c-Met/HGF receptor in rat brain: implication as neurotrophic factor. Brain Res Mol Brain Res 32:197–210
13. Howland DS, Liu J, She Y, Goad B, Maragakis NJ, Kim B, Erickson J, Kulik J, DeVito L, Psaltis G, DeGennaro LJ, Cleveland DW, Rothstein JD (2002) Focal loss of the glutamate transporter EAAT2 in a transgenic rat model of SOD1 mutant-mediated amyotrophic lateral sclerosis (ALS). Proc Natl Acad Sci USA 99:1604–1609
14. Kato S, Shimoda M, Watanabe Y, Nakashima K, Takahashi K, Ohama E (1996) Familial amyotrophic lateral sclerosis with a two base pair deletion in superoxide dismutase 1 gene: multi-system degeneration with intracytoplasmic hyaline inclusions in astrocytes. J Neuropathol Exp Neurol 55:1089–1101
15. Kato S, Hayashi H, Nakashima K, Nanba E, Kato M, Hirano A, Nakano I, Asayama K, Ohama E (1997) Pathological characterization of astrocytic hyaline inclusions in familial amyotrophic lateral sclerosis. Am J Pathol 151:611–620
16. Kato S, Takikawa M, Nakashima K, Hirano A, Cleveland DW, Kusaka H, Shibata N, Kato M, Nakano I, Ohama E (2000) New consensus research on neuropathological aspects of familial amyotrophic lateral sclerosis with superoxide dismutase 1 (SOD1) gene mutations: inclusions containing SOD1 in neurons and astrocytes. ALS Other Motor Neuron Disord 1:163–184
17. Kato S, Nakashima K, Horiuchi S, Nagai R, Cleveland DW, Liu J, Hirano A, Takikawa M, Kato M, Nakano I, Sakoda S, Asayama K, Ohama E (2001) Formation of advanced glycation end-product-modified superoxide dismutase-1 (SOD1) is one of the mechanisms responsible for inclusions common to familial amyotrophic lateral sclerosis patients with SOD1 gene mutation, and transgenic mice expressing human SOD1 gene mutation. Neuropathology 21:67–81
18. Kato T, Hirano A, Kurland LT (1987) Asymmetric involvement of the spinal cord involving both large and small anterior horn cells in a case of familial amyotrophic lateral sclerosis. Clin Neuropathol 6:67–70
19. Kurland LT, Mulder DW (1955) Epidemiologic investigations of amyotrophic lateral sclerosis. II. Familial aggregations indicative of dominant inheritance. Neurology 5:249–268
20. LoPachin RM Jr, Aschner M (1993) Glial-neuronal interactions: relevance to neurotoxic mechanisms. Toxicol Appl Pharmacol 118:141–158
21. Maina F, Klein R (1999) Hepatocyte growth factor, a versatile signal for developing neurons. Nat Neurosci 2:213–217
22. Maina F, Hilton MC, Andres R, Wyatt S, Klein R, Davies AM (1998) Multiple roles for hepatocyte growth factor in sympathetic neuron development. Neuron 20:835–846
23. Matsumoto K, Nakamura T (1997) HGF: its organotrophic role and therapeutic potential. Ciba Found Symp 212:198–211; discussion 211–214
24. Nakamura T, Nawa K, Ichihara A (1984) Partial purification and characterization of hepatocyte growth factor from serum of hepatectomized rats. Biochem Biophys Res Commun 122:1450–1459
25. Nakamura T, Nishizawa T, Hagiya M, Seki T, Shimonishi M, Sugimura A, Tashiro K, Shimizu S, Kazama T, Isemura M, Sato Y (1989) Molecular cloning and expression of human hepatocyte growth factor. Immunohistochemical localization of heparan sulfate-containing proteoglycan in normal human skin with monoclonal antibodies: comparison with that of fibronectin. Nature 342:440–443
26. Nakano I, Hirano A, Kurland LT, Mulder DW, Holley PW, Saccomanno G (1984) Familial amyotrophic lateral sclerosis. Neuropathology of two brothers in American "C" family. Neurol Med (Tokyo) 20:458–471
27. Novak KD, Prevette D, Wang S, Gould TW, Oppenheim RW (2000) Hepatocyte growth factor/scatter factor is a neurotrophic survival factor for lumbar but not for other somatic motoneurons in the chick embryo. J Neurosci 20:326–337
28. Okura Y, Arimoto H, Tanuma N, Matsumoto K, Nakamura T, Yamashima T, Miyazawa T, Matsumoto Y (1999) Analysis of neurotrophic effects of hepatocyte growth factor in the adult hypoglossal nerve axotomy model. Eur J Neurosci 11:4139–4144
29. Park M, Dean M, Kaul K, Braun MJ, Gonda MA, Vande Woude G (1987) Sequence of MET protooncogene cDNA has features characteristic of the tyrosine kinase family of growth-factor receptors. Proc Natl Acad Sci USA 84:6379–6383
30. Rothstein JD, Martin LJ, Kuncl RW (1992) Decreased glutamate transport by the brain and spinal cord in amyotrophic lateral sclerosis. N Engl J Med 326:1464–1468
31. Rothstein JD, Van Kammen M, Levey AI, Martin LJ, Kuncl RW (1995) Selective loss of glial glutamate transporter GLT-1 in amyotrophic lateral sclerosis. Ann Neurol 38:73–84
32. Schmitt A, Asan E, Puschel B, Jons T, Kugler P (1996) Expression of the glutamate transporter GLT1 in neural cells of the rat central nervous system: non-radioactive in situ hybridization and comparative immunocytochemistry. Neuroscience 71:989–1004
33. Shibata N, Hirano A, Kobayashi M, Siddique T, Deng HX, Hung WY, Kato T, Asayama K (1996) Intense superoxide dismutase-1 immunoreactivity in intracytoplasmic hyaline inclusions of familial amyotrophic lateral sclerosis with posterior column involvement. J Neuropathol Exp Neurol 55:481–490
34. Silani V, Ciammola A, Pizzuti A, Cardin V, Scarlato G (1999) Motor neurone metabolism. J Neurol Sci 169:161–169
35. Sun W, Funakoshi H, Nakamura T (2002) Overexpression of HGF retards disease progression and prolongs life span in a transgenic mouse model of ALS. J Neurosci 22:6537-6548
36. Takahashi K, Nakamura H, Okada E (1972) Hereditary amyotrophic lateral sclerosis. Histochemical and electron microscopic study of hyaline inclusions in motor neurons. Arch Neurol 27:292–299
37. Tower DB (1992) A century of neuronal and neuroglial interactions, and their pathological implications: an overview. Prog Brain Res 94:3–17
38. Trotti D, Rolfs A, Danbolt NC, Brown RH Jr, Hediger MA (1999) SOD1 mutants linked to amyotrophic lateral sclerosis selectively inactivate a glial glutamate transporter. Nat Neurosci 2:427–433
39. Van Bockstaele EJ, Colago EE (1996) Selective distribution of the NMDA-R1 glutamate receptor in astrocytes and presynaptic axon terminals in the nucleus locus coeruleus of the rat brain: an immunoelectron microscopic study. J Comp Neurol 369:483–496
40. Yamamoto Y, Livet J, Pollock RA, Garces A, Arce V, de Lapeyriere O, Henderson CE (1997) Hepatocyte growth factor (HGF/SF) is a muscle-derived survival factor for a subpopulation of embryonic motoneurons. Development 124:2903–2913